INTEGRATED USE OF SURFACE-GEOPHYSICAL METHODS TO INDICATE SUBSURFACE FRACTURES AT MILFORD, NEW HAMPSHIRE

By D.A. Lieblich, F.P. Haeni, and J.W. Lane, Jr.

U.S. GEOLOGICAL SURVEY

Water-Resources Investigations Report 92-4056

Prepared in cooperation with the

U.S. ENVIRONMENTAL PROTECTION AGENCY

Hartford, Connecticut
1992

U.S. DEPARTMENT OF THE INTERIOR

MANUEL LUJAN, JR., Secretary

U.S. Geological Survey

Dallas L. Peck, Director

For additional information
write to:

Chief, Connecticut Office
U.S. Geological Survey
450 Main Street, Room 525
Hartford, CT 06103

Copies of this report can
be purchased from:

U.S. Geological Survey
Books and Open-File Reports Section
Federal Center, Box 25425
Denver, CO 80225

CONTENTS

ILLUSTRATIONS

ILLUSTRATIONS (continued)

CONVERSION FACTORS AND VERTICAL DATUM

Multiply	by	To obtain
centimeter (cm)	0.3937	inch
meter (m)	3.281	foot
kilometer (km)	0.6214	mile
kilometer per hour (km/hr)	0.6214	mile per hour
kilometer per second (km/s)	3,281	foot per second
meter per nanosecond (m/ns)	3.281	foot per nanosecond
millisiemen per meter (mS/m)	0.305	millisiemen per foot
ohm-meter (ohm-m)	3.281	ohm-foot

Sea level--In this report "sea level" refers to the National Geodetic Vertical Datum of 1929 (NGVD of 1929)- a geodetic datum derived from a general adjustment of the first-order level nets of both the United States and Canada, formerly called "Sea Level Datum of 1929."

INTEGRATED USE OF SURFACE-GEOPHYSICAL METHODS TO INDICATE SUBSURFACE FRACTURES AT MILFORD, NEW HAMPSHIRE

by D.A. Lieblich, F.P. Haeni, and J.W. Lane, Jr.

ABSTRACT

Four surface-geophysical methods were used to indicate the presence and estimate the orientations of subsurface fractures at a site in Milford, New Hampshire. The methods used were ground-probing radar, inductive terrain conductivity, direct-current resistivity, and seismic refraction.

Three of the four geophysical data sets contain anomalies that are interpreted as representing subsurface fracturing. Interpretation of the individual data sets yields some conflicting results; however, an integrated interpretation indicates one fracture set that trends northeast and possibly a second set that trends northwest. These local fracture orientations are consistent with mapped regional orientations found in previous studies. Ground-probing radar data contain reflections from the bedrock surface and from the internal structure of the glacial and postglacial deposits overlying the bedrock, but evidence of bedrock fractures is not seen. Inductive terrain-conductivity data show anomalies that are interpreted as being caused by one fracture or fracture zone that trends in a northeast direction and possibly two additional fractures or fracture zones that trend northwest. Direct-current resistivity data show anomalies that are interpreted as being caused by a fracture set that trends north-northeast and possibly a second fracture set that trends generally west-northwest. A fracture set that trends northeast is interpreted from the seismic-refraction data.

INTRODUCTION

Bedrock with normally low, primary permeability may be capable of substantial fluid transport if it is fractured. These fractures can act as conduits through the bedrock, and, because their orientations are not usually random, they may introduce a significant anisotropy to the subsurface flow pattern. Surface-geophysical methods can indicate the orientations of subsurface fractures and thereby provide data that may also indicate a preferred flow direction.

A study was undertaken by the U.S. Geological Survey (USGS), in cooperation with the U.S. Environmental Protection Agency (USEPA), to determine whether integrated surface-geophysical methods could indicate the presence and estimate the orientations of steeply dipping subsurface fractures at a site in Milford, New Hampshire (fig. 1). The study area is near a USEPA Superfund site where hazardous fluids have been found in both the overburden and bedrock. Regional geologic data indicate the presence of fractured bedrock. Characterization of the fluid transport properties of the subsurface at this site is of primary importance in assessing the occurrence and movement of contamination, as well as in developing methods for limiting or alleviating such contamination.

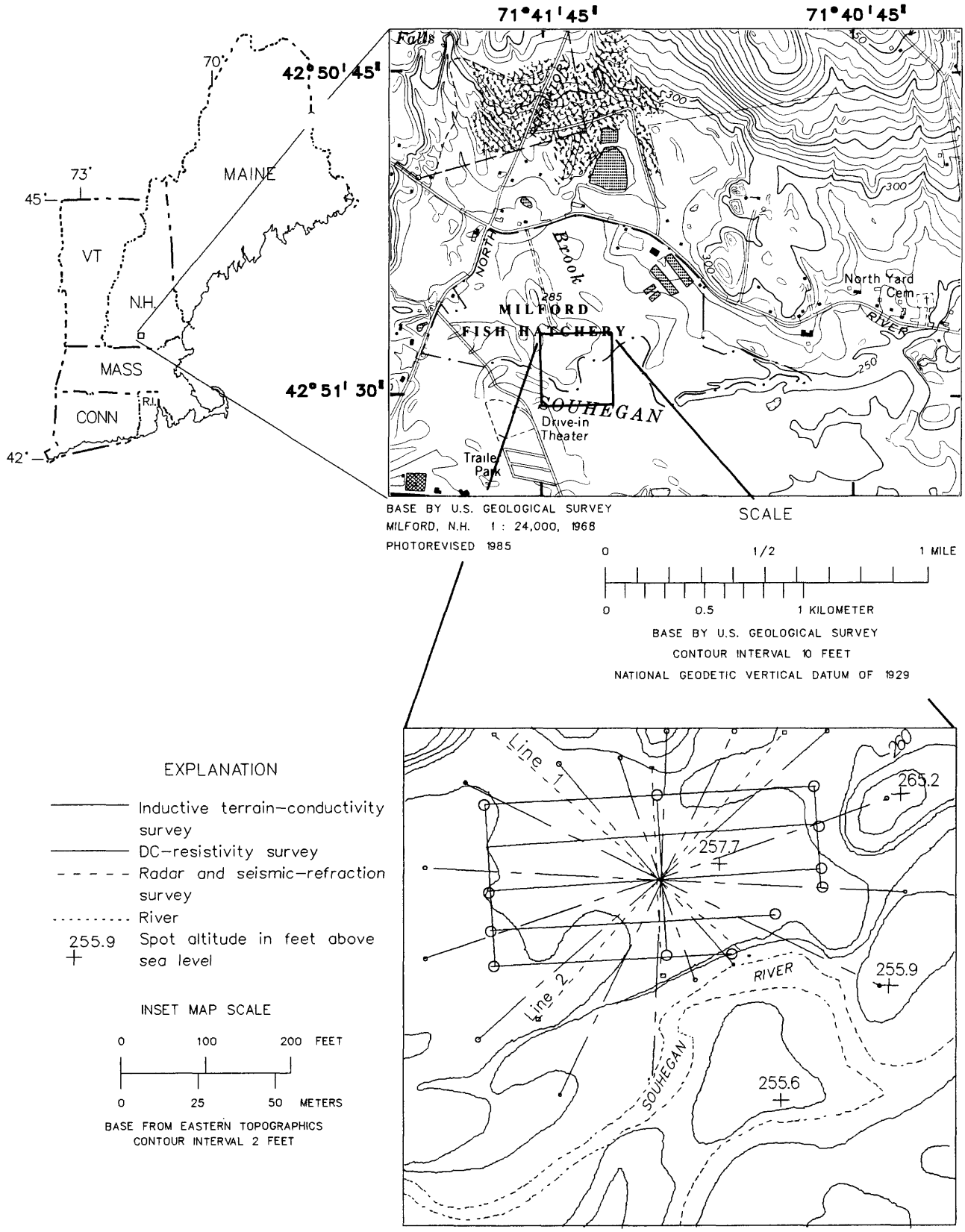

Figure 1.--Location of study area and geophysical surveys.

Purpose and Scope

This report (1) presents the results of a surface-geophysical study to evaluate whether surface-geophysical methods could be used to indicate the presence and estimate the orientations of steeply dipping subsurface fracture zones at a site near Milford, New Hampshire; and (2) provides information (derived from the individual and combined interpretation of the geophysical data sets) useful for site characterization and remediation.

A review of previous studies, which provides a description of the study area, is followed by a brief summary of each surface-geophysical method used in this study. A general description of the approach to geophysical investigations at this site follows. For each method, details of the data acquisition precede the data presentation.

A thorough assessment of the problems associated with using surface-geophysical methods for subsurface fracture detection is beyond the scope of this report. This report is restricted to a description of the application of relatively standard and readily available surface-geophysical methods.

Description of the Study Area and Previous Investigations

The study area is located on the northern bank of the Souhegan River in the town of Milford, New Hampshire (fig. 1). The site is covered with 3 to 12 m of glacial and postglacial deposits that are of variable thickness. A discontinuous till layer is present at the base of these deposits. The crystalline bedrock is fractured, and the closest outcrop is 0.5 km away.

The study area has been described in the following three reports: (1) a report by BCI Geonetics (1984) on bedrock fracture analysis; (2) a report by the USEPA (1985), identifying the chemical contaminants found at the Savage and Keyes municipal well sites and the regional fracture patterns based on a photolineament study; and (3) a report by the Hydrological Investigation Unit of the New Hampshire Water Supply and Pollution Control Commission (NHWSPCC) (1985) that includes a local geologic overview, as well as interpretation of data collected by seismic refraction, direct-current (DC) resistivity, and electromagnetic (EM) surveys.

Geologic Data

An outcrop study of fractures at seven different localities in the Milford area is included in the BCI Geonetics report (1984). The results show a north-northeast (NNE)-trending joint set to be the most persistent in this region. These fractures are observed to form discrete fracture zones, approximately 12 m in width, with individual joint spacing increasing from 5 to 10 cm at the zone center to an unspecified distance at the edge. On a larger scale, the fractures are not regularly spaced. In addition, these fractures were observed to be "open, oxidized, and water bearing". Stewart (1964) also showed a high correlation between the NNE trend, topographic lows, and high-yield water wells in the neighboring town of Hollis. An east-southeast (ESE)-trending joint set and a less well developed north-northwest (NNW)-trending set were also observed. All three joint sets are presumed to be subvertical; their actual dips are not given in any of the reports. It is possible that the ESE set may dip as low as 60° (degrees) if this set is actually an array of high-angle reverse faults, as postulated in the BCI Geonetics (1984) report. Horizontal fractures, which increased in spacing with increasing depth, were observed to a depth of 7.6 m in quarry walls. A summary of the strike frequency of measured outcrop fractures as a function of azimuth is shown in figure 2.

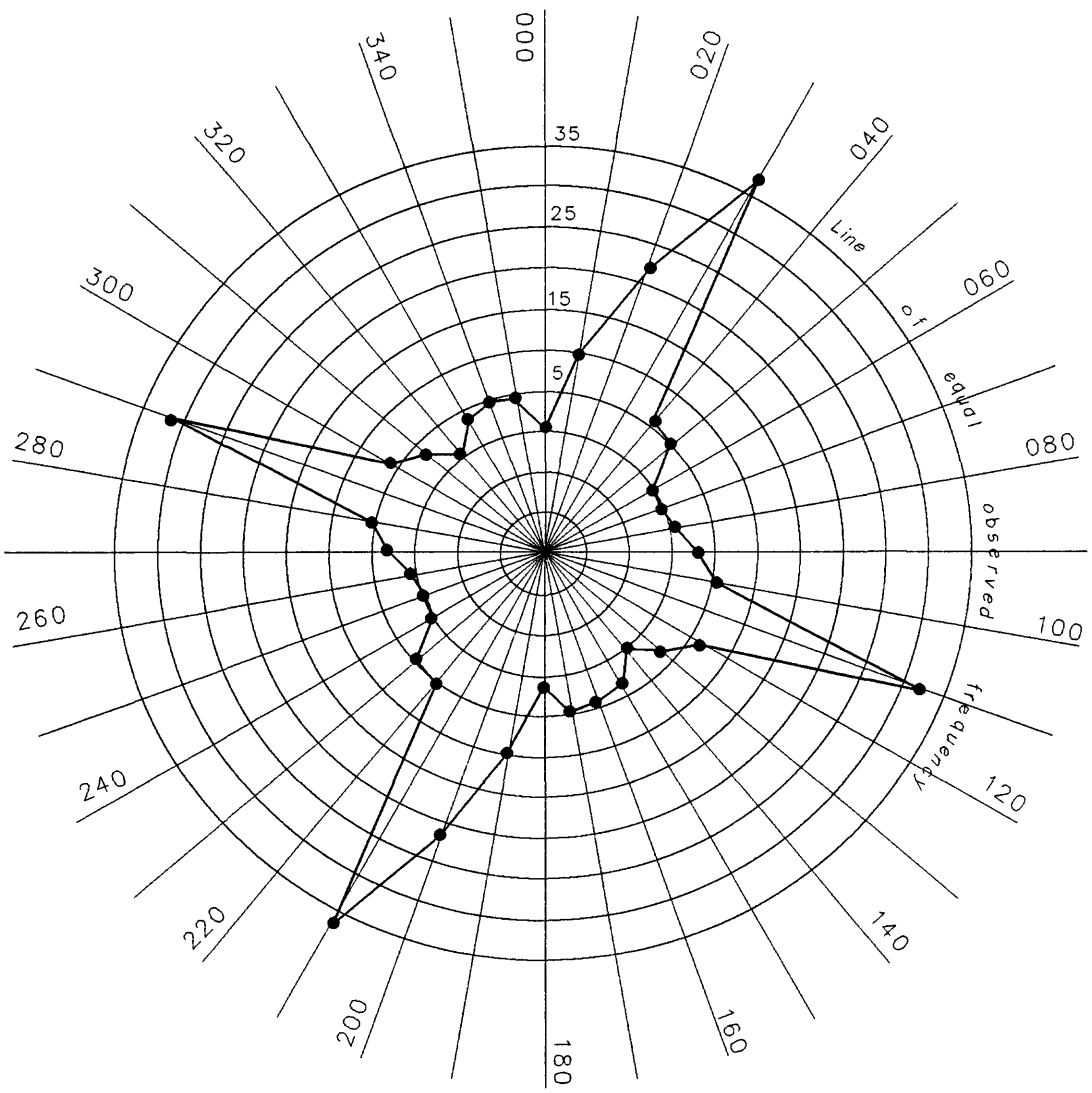

EXPLANATION

000.0 Degrees from magnetic north

● Fracture strike frequency measured in outcrop

Figure 2.--The strike frequency of measured outcrop fractures as a function of azimuth. (Modified from BCI Geonetics, 1984, fig. 3.)

The BCI Geonetics and the USEPA reports also contain photolineament interpretations. Three distinct trends were recognized in the BCI Geonetics report: NNE, ESE, and NNW. The ESE-trending lineaments were "most persistently expressed" on the photos.

No geologic data on the orientation and extent of foliation are available from the study site; this adds a degree of uncertainty to the geophysical interpretation of the occurrence and orientation of fracturing. Interpretation of fractures from geophysical data sets depends upon being able to differentiate fracture responses from the responses of other planar features, such as foliation.

Geophysical Data

Seismic refraction, DC resistivity, and electromagnetic data interpretations contained in the NHWSPCC report are of limited use for the present investigation, because the purpose of those surveys was to delineate the subsurface layer boundaries and indicate water-quality changes. The electrical methods were not used in a manner capable of detecting bedrock fractures at this site. The interpretation of fractures from single line, seismic-refraction delay times is a speculative procedure. Use of bedrock topography as an indication of fracture zones is indirect and suspect unless correlated with some other data. The seismic-refraction data did however provide an indication of the gross subsurface layer boundaries (bedrock is generally shallower than 15 m and is locally as shallow as 3 m). Seismic velocities for the saturated unconsolidated material are about 1.5 km/s and seismic velocities for bedrock are about 4.5 km/s.

PRINCIPLES OF SURFACE-GEOPHYSICAL METHODS

A brief review of the surface-geophysical methods used in this study is given below. These methods are ground-probing-radar (GPR), inductive terrain conductivity, DC resistivity, and seismic refraction. The order of discussion is from the fastest to the slowest method in terms of data-collection time in the field. Although the order is not intended to indicate how a field program should be designed, it does represent one way of designing such a program.

Ground-Probing Radar

GPR uses transmitter and receiver antennae, which may be the same unit, to generate and detect subsurface EM waves. Measurable signals can be obtained when the EM wave encounters changes to any individual or combination of the following physical properties: conductivity, dielectric permittivity, and magnetic permeability. The advantage of GPR for fracture detection is that the conductivity and dielectric permittivity usually change significantly in a fluid-saturated fracture or fracture zone compared to the properties in the host rock. The image of a fracture on a radar section can range from a sublinear coherent event[1/] to a diffraction hyperbola with a "ringy" appearance. Discontinuous layers or foliation, as well as localized, small scatters, can also produce sublinear coherent events and diffraction hyperbolas.

1/ As used in this report, an event is "a lineup on a number of traces which indicates the arrival of new seismic energy...May indicate a reflection, refraction, diffraction, or other type of wavefront."

In previous investigations, at other sites, Ulriksen (1982) obtained reflections from individual fractures or fracture zones in granodiorite. Imse and Levine (1985) obtained strong scattering responses from steeply dipping fractures in carbonate rocks in northern New York. Olsson and others (1988) obtained reflections in crystalline rocks from steeply dipping individual fractures with a borehole radar unit.

In addition to the possibility of detecting signals from individual fractures or fracture zones directly, GPR can also be used to map the depth to bedrock and changes in the overburden. These data can be used to reduce the ambiguity in seismic-refraction interpretations. In shallow studies, the bedrock-overburden interface usually represents a significant contrast in elastic and electric properties thus generating a radar reflection as well as refracted and reflected seismic waves. If radar-velocity information is available or is measured, the radar image can be used to determine the thickness of material above the interface.

Inductive Terrain Conductivity

Two coils, a transmitter and a receiver, are used in the inductive terrain-conductivity method. Alternating current flowing in the transmitter coil causes a primary magnetic field. This magnetic field induces eddy currents in the subsurface, which, in turn, cause a secondary magnetic field. The receiver coil measures the ratio of the secondary magnetic field to the primary magnetic field. In general, the EM field responds to changes in conductivity, dielectric permittivity, and magnetic permeability. Changes in the magnetic permeabilities of rocks are generally negligible, and, because of the low frequency of the signal used, displacement currents caused by the dielectric properties of the medium are also negligible. Measurements are, therefore, sensitive to changes in the conductivity of the subsurface.

A mobile source is used in the inductive terrain-conductivity method, and allows dipping fractures of any strike to be detected. In addition, operation under the low-induction-number assumption (McNeill, 1980a) permits the depth of penetration to be varied by changing the operating frequency and the intercoil spacing. Orienting the two coils either vertically or horizontally causes preferential sensitivity in the instrument response to subsurface structures with different orientations. Sensitivity to vertical or near vertical conductors, such as fluid-filled fractures, is obtained by orienting the coils horizontally (the vertical dipole mode) (McNeill, 1980b, fig. 6). In this orientation, the image of a subsurface vertical conductor is a symmetric waveform centered over the conductor and with a peak to peak distance equal to two coil spacings. If this method is used in areas with conductive overburden, small increases in the thickness of the conductive overburden can cause anomalies similar in size and shape to those caused by vertical conductors (Villegas-Garcia and West, 1983).

Successful use of the method for fracture detection, using the coils in the vertical dipole mode, has been demonstrated by Palacky and others (1981) and by van Lissa and others (1987) in fractured granitic rocks where faults

and fracture zones were identified on aerial photographs. In addition, a recent study in carbonate rocks by Yager and Kappel (1988) has demonstrated the use of an inductive terrain-conductivity instrument (Geonics EM-34[2/]) for high-angle fracture detection in sedimentary rocks.

Direct-Current Resistivity

The DC-resistivity method uses either a DC current or an alternating current with a frequency commonly below 10 Hz (Hertz). The method is commonly applied by sending current into the ground through two electrodes and measuring the potential difference (voltage) at two other electrodes. The apparent resistivity (resistivity of a homogeneous, isotropic volume of earth) is estimated for a specific electrode spacing and geometry. Ideally, the apparent resistivity is independent of measured voltage and input current; however, the presence of ambient noise often causes deviations. The DC-resistivity method measures the apparent resistivity of a volume of rock, which is usually large compared to the scale of the spacing between individual fractures or fracture zones. This may require the rock to be treated as an anisotropic medium and increases the scope and complexity of the interpretation.

The DC-resistivity method is especially useful in differentiating rock units with varying resistivities, and its depth of penetration is controlled primarily by the spacing of the current electrodes. Near surface and three-dimensional effects are inherent in real data, and normal interpretive methods do not account for them. The most common application of the DC-resistivity method for the detection of fractures in rock is to identify and correlate low-resistivity zones in a grid of resistivity traverses. Rotation of linear arrays (either Wenner or Schlumberger) has also been used to identify the presence of small but pervasive fractures that cause an anisotropic bulk resistivity. It should be noted that the interpretation of azimuthal resistivity data is not intuitive--for a single set of oriented subvertical fractures, the apparent resistivity maximum corresponds to the orientation of the fractures with the apparent resistivity minimum oriented orthogonally. However, the orientation of the fractures is also the true resistivity minimum. This phenomenon is known as the "paradox of anisotropy" (Keller and Frischknecht, 1966, p. 103). Azimuthal resistivity measurements over a layered subsurface can also produce an anisotropic bulk resistivity, if the layering is not parallel to the surface on which measurements are made.

Successful detection of fractures using azimuthal DC-resistivity surveys has been demonstrated in the following studies: Risk (1975) in volcanic rocks; McDowell (1979) in granitic rocks overlain by fluvial sediments; Palacky and others (1981) in fractured granitic rocks associated with faults and fracture zones identified on aerial photographs; Soonawala and Dence (1981) in granitic rocks; Taylor (1982) in carbonates overlain by till; Mallik and others (1983) in granites, amphibolites, and metabasic rocks; Leonard-Mayer (1984a, 1984b) in carbonate rocks overlain by up to 2 m of soil or glacial deposits; Ogden and Eddy (1984) in carbonate rocks; Taylor (1984) in carbonates overlain by till; and Taylor and Fleming (1988) in gabbro, basalt, dolomite, and till.

[2/] Use of trade names is for identification purposes only and does not constitute endorsement by the U.S. Geological Survey.

Seismic Refraction

The seismic-refraction method uses an impulsive source to generate elastic waves that propagate through the subsurface. In standard applications, a compressional wave (p-wave) is used, although shear waves (s-waves) may also be used. The critically refracted (head) wave, either p or s, is detected as a strong change in particle velocity (or acceleration) at geophones on the surface when there is a seismic velocity increase at depth. For constant velocity layers, there is a linear change in arrival time as a function of detector distance. This change can be used to obtain the velocity at which the head wave travels through the medium. For a homogeneous, isotropic medium, the velocity is a function of the density, compressibility, and shear modulus of the medium.

The effects of single fractures or small isolated fracture zones are unlikely to be seen in p-wave refraction surveys of any kind because the velocity and (or) attenuation changes caused by these objects are normally too small to be detected. Azimuthal refraction methods can detect an anisotropic distribution of pervasive fractures in the bulk rock. For a single subvertical fracture set, a velocity maximum occurs along the strike direction, and a velocity minimum occurs orthogonal to the strike direction. Velocity and (or) thickness inhomogeneities in the material overlying the reflector can also generate an anisotropic azimuthal velocity function.

P-wave refraction experiments that have successfully detected fractures include: Bamford and Nunn (1979) and Crampin and others (1980) in carbonate rocks; Park and Simmons (1982) in granites, quartz syenites, and volcanic rocks with glacial overburden; and Imse and Levine (1985) in carbonate rocks with glacial overburden.

APPROACH

Fractures represent discontinuities in an otherwise continuous and, in the simplest case, homogeneous body of rock. If fractures are inhomogeneously and (or) anisotropically distributed throughout a rock body, the physical properties of the bulk rock may require mathematical formulations that consider the rock body to be either inhomogeneous, anisotropic, or both. These topics remain at the forefront of geophysical research (Frazer, 1990; Wait, 1990). Existing, simple theories can be used to interpret geophysical methods that are sensitive to rock physical properties at wavelengths comparable to the size of individual fractures or fractures zones.

Despite the developmental state of theoretical ideas, observational data from experimental and field studies have been, and continue to be, successfully collected (see individual methods in previous section). The basic conclusion that can be drawn from most of these investigations is that the change in the bulk physical properties of the rock caused by fracturing is generally small. Therefore, for each method, great care must be exercised during survey design and data collection to minimize all effects that could interfere with and (or) mask the effects of fractures.

Interferences from various natural or cultural sources may mask or seriously degrade the data and decrease the possibility of detecting a clear fracture response. Although filtering techniques can be applied, they are seldom perfect and may be inappropriate for weak signals, emphasizing the importance of obtaining as many independent data sets as possible. Constrained interpretation of these data sets through either a simple, manual cross correlation (integration), as is done here, or through a complex, integrated inversion technique should improve confidence in the results and perhaps improve resolution over what could be obtained by use of a single method.

The design of each surface-geophysical survey considered all available information on strength, spatial orientation, size, and shape of the expected physical property anomaly, as well as the distance from the source of the anomaly to the detectors. Residual contaminants are assumed to have a negligible effect on the bulk physical properties, as measured by the methods used in this study, because of their very small concentrations.

Optimal survey design considered not only the detection of individual geophysical anomalies, but also the interpretation of different geophysical data. This additional consideration arose because of the desire to integrate the interpretational results of the different methods. Optimal survey design was implemented by requiring that at least some of the data points from the different survey grids coincided. Ultimately, a compromise was struck between the economically defined grids, the optimal survey design, and site logistics.

Data were collected in an open field, on the north side of the Souhegan River (fig. 1). Four radar lines, coincident with four radiating seismic-refraction lines, at azimuths of southeast (SE), southwest (SW), east (E), and north (N), were collected. Eight DC-resistivity lines, spaced 22.5° apart in azimuth, starting at north, were also collected. Inductive terrain-conductivity data were collected on a grid consisting of five lines striking east, three lines striking north, and two additional lines striking NE and NW.

INTEGRATED USE OF SURFACE-GEOPHYSICAL METHODS TO INDICATE FRACTURES

GPR, inductive terrain-conductivity, DC-resistivity, and compressional-wave seismic-refraction data sets collected at Milford, New Hampshire are presented in this section. Details of data acquisition for each method are presented first; this is followed by observations and interpretations for each data set.

Ground-Probing Radar

A radar unit manufactured by Geophysical Survey Systems Inc. (GSSI) was used in the survey. A bistatic antenna configuration operating at a center frequency of 80 MHz (megahertz) was used. The antennae were towed about 30 m behind a vehicle moving at approximately 4.8 km/hr. Recordings were made at a scan rate of 25.6 scans per second and a time scale range of 700 ns (nanoseconds). The range gain was adjusted in the field and recorded to allow for a more appropriate adjustment during processing. Records were marked for every 6.1 m of ground covered, and two-way travel time was printed on the records. Of four lines collected, only the two lines that present the clearest picture of the subsurface are discussed. The SE-NW line, referred to as line 1, is shown in figure 3, and the SW-NE line,

referred to as line 2, is shown in figure 4. A copy of an original field record is shown in figure 3. Marks are not equally spaced because the speed with which the radar unit was towed over the ground varied: Higher than "normal" speed causes compression of the horizontal axis and lower than "normal" speed causes extension of the horizontal axis. The radar section shown in figure 4 has been corrected for this variation. The horizontal scale is approximately four times as long as the vertical scale, after depth conversion of the latter; steeply dipping reflectors on the radar record correspond to almost flat reflectors within the Earth.

The data were processed using GSSI's RADAN processing package. High and low pass (horizontal and vertical) filters were applied. No significant enhancement of the radar sections, both in general and for specific reflection events, was evident and therefore no further noise processing was done. Some interpretive processing was performed--all four sections were displayed in color, and "attribute sections" showing the different attributes of the Hilbert Transform of each section were produced. These sections were found to be helpful in correlating events laterally along a section.

Three basic subsurface layers were interpreted from the cylindrical volume enclosed by all four sections--an upper layer consisting of many continuous reflectors; a middle layer with a strong reflector at its top and almost no signal in the middle of the section (where it is thickest); and bedrock. Using the surficial geologic map of the area (Koteff, 1970), the upper layer is interpreted as an alluvial flood-plain deposit containing continuous reflectors, and the middle layer is interpreted as a coarse-grained ice-contact deposit that becomes increasingly finer grained with depth. The boundaries of these layers are not continuously traceable on individual sections, however, interpretation based on a three-dimensional fence diagram indicates that the three layers are represented throughout the study area. A separate till layer, expected to overlie the bedrock, could not be distinguished on the radar records. The water table, which was measured at depths between 1.5 and 2.1 m in seismic shot holes, is interpreted on the sections to be the reflection arriving around 30 ns.

Line 1- Observations and Interpretations

1. Observation: An event that dips to the southeast and undulates slightly is present at about 210 ns on the southeastern end of the section.

   Interpretation: The base of what is interpreted to be an alluvial flood-plain deposit corresponds to the event at about 210 ns on the southeastern end of the section. Using an assumed velocity of 0.12 m/ns for the unsaturated zone (Johnson, 1987), known to be about 2 m thick from drill holes, and 0.06 m/ns for the saturated stratified drift (Beres and Haeni, 1991), the depth of the event is 7.5 m.

2. Observation: A second event that may dip slightly to the northwest is seen at about 350 ns on the southeastern end of the section.

   Interpretation: The top of the bedrock corresponds to the event at about 350 ns on the southeastern end of the section. Using assumed velocities as above, the depth to bedrock is 11.6 m. The increasing slope of the bedrock event between the first and the fifth marks on the line may indicate scattering from an inhomogeneity above, below, or on the bedrock surface, or, alternatively, it may delineate a change in dip of the bedrock itself.

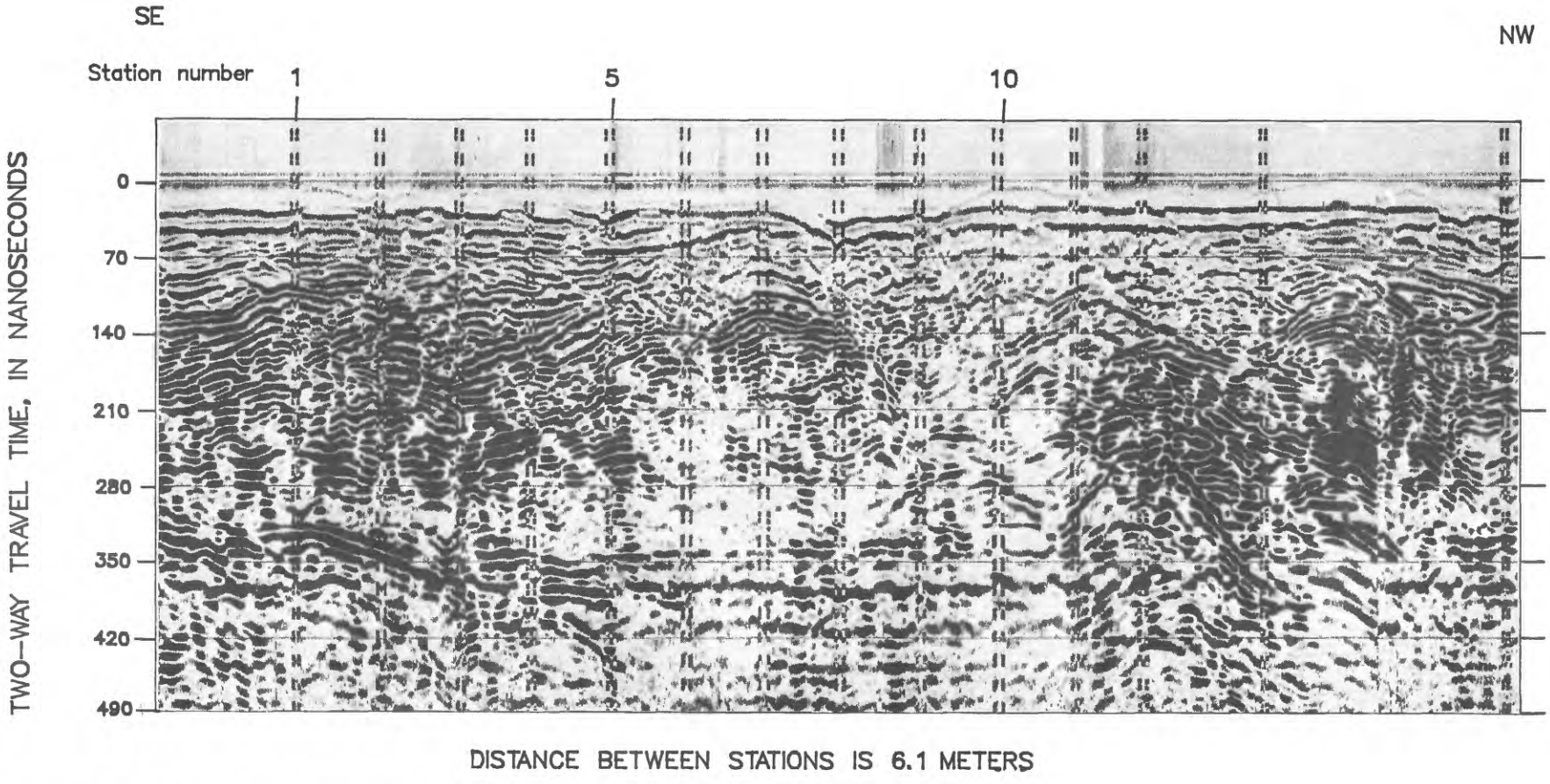

Figure 3.--Southeast-northwest ground-probing radar section (along line 1). Distance between stations appears variable on the section because of different towing speeds.

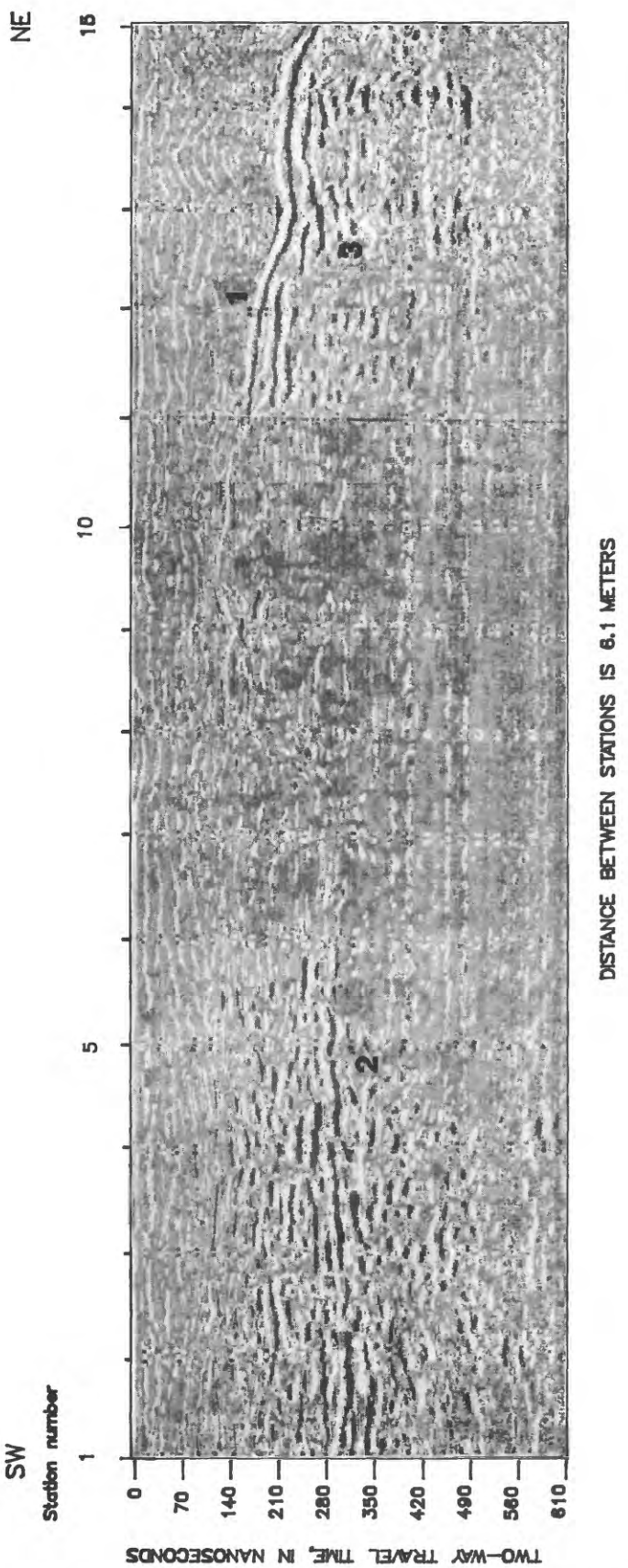

Figure 4.--Southwest-northeast ground-probing radar section (along line 2).

3. Observation: Between these two major events, some discontinuous events from possibly flat-lying reflectors occur. Signal strength is low near the center of the section.

   Interpretation: The discontinuous events between the interpreted alluvial flood-plain deposit and the bedrock occur within the middle layer that is interpreted as an ice-contact deposit that becomes increasingly finer grained with depth. Increased signal attenuation near the center of the line, where the middle layer is thickest, is consistent with this interpretation, if the clay content increases as the amount of fine-grained material increases.

4. Observation: On the northwestern end of the section, a number of discontinuous, dipping, and often strong events are present from 140 to 420 ns.

   Interpretation: Boulders and (or) discontinuous lithologic lenses within this layer could cause these events.

Line 2- Observations and Interpretations

1. Observation: A strong event is present at about 210 ns on the northeastern end of the section and undulates upward towards 70 ns at the southwestern end or decreases to 280 ns on the southwestern end.

   Interpretation: The undulating event at about 210 ns on the northeastern end of the section is interpreted to be the contact between the alluvial flood-plain deposit and the ice-contact deposit. This contact probably correlates with the event at 70 ns (5.2 m) on the southwestern end of the section. The base of the alluvial layer, at about 100 ns around mark 8, could also correlate to the event at about 280 ns around mark 6. Interference seen between marks 7 and 8 is probably caused by edge diffractions. Such diffractions may be the result of a reflectivity change caused by a geologic facies change and (or) a rapid thickness change.

2. Observation: A relatively flat and continuous event at about 280 ns is present on the southwestern end of the section. The event dips to the northeast between marks 6 and 8, despite the disruption by what appears to be interference caused by scattering from a possible end or change in the overlying event, and may be traceable to 420 ns on the northeastern end of the section.

   Interpretation: The top of the bedrock corresponds to the relatively flat and continuous event at about 280 ns. Between marks 6 and 8, the bedrock reflection is interpreted to dip to the northeast despite the fact that the reflection is slightly disrupted by the interference noted above. Alternatively, this dipping event could be an edge diffraction caused by truncation of the reflector against a fault. The extension of the bedrock reflector on the northeastern end of the section is seen around 420 ns.

3. Observation: Some discontinuous, strong, and subhorizontal events are present below the undulating event, on the northeastern end of the section between about 280 and 420 ns.

Interpretation: Discontinuous events above the bedrock may represent boulders and (or) discontinuous lithologic or saturation lenses within an ice-contact layer.

4. Observation: Signal strength is low near the center of the section.

   Interpretation: Increased signal attenuation near the center of the line, where the intermediate layer would be thickest, is consistent with the interpretation of an intermediate ice-contact layer with some silt and clay present in it.

Inductive Terrain Conductivity

Inductive terrain-conductivity data, consisting of both horizontal and vertical dipole measurements, were collected using the EM-34, a Slingram type dual-loop instrument, manufactured by Geonics Inc. Five lines striking east were collected 15.2 m apart (fig. 5). Two lines, one striking northeast and one northwest (fig. 6), from the center of the grid, and three lines striking north (fig. 7) were also collected. A station spacing of 3.0 m and a coil separation of 20 m was used on the east and north lines, and a 6.1-m station spacing was used on the northeast and northwest lines. The coil separation was always parallel to the line.

Field measurements could be read to ±0.2 mS (millisiemen) or better. Where unstable readings were obtained, multiple readings were made and if necessary, stations were reoccupied at later times. The lines were collected over a number of days separated by as much as 4 months, therefore, the background EM field varies within the data set and may be the cause of single point conductivity mismatches.

Contributions to the noise included atmospheric effects, which could generally be eliminated because of the obvious long period drift in the meter readings at a given station; possible soil moisture variations (W.M. Kappel, U.S. Geological Survey, written commun., 1990); and (or) manmade interference from a well just north of the field.

Observations and Interpretations

The characteristic signature of a buried vertical conductor, which is thin compared to the coil separation, is a symmetric waveform. A conductivity minimum is centered over the conductor, which may be a fracture or fracture zone, and has a period of about two coil spacings from peak to peak. This signature is obtained using the vertical dipole, on a traverse line collected perpendicular to the strike of the conductor and with the coil separation along the line (Nair and others, 1968). When the traverse is not oriented perpendicular to the strike of the conductor, the waveform is different: the amplitude decreases as the angle between the strike of the conductor and the direction of the coil separation decreases. A cross-correlation procedure was used to interpret the data. First, the locations of probable and possible anomalies were identified on individual lines by cross correlating the data with a waveform of the correct shape and wavelength, for the given coil separation, and assuming a traverse orthogonal to the strike of a subsurface conductor. Then, anomalies and their trends were analyzed on the east lines by cross correlation of adjacent pairs of lines. A composite of all the horizontal- and vertical-dipole data collected at the site, with probable and possible anomalies, as well as interpreted fracture orientations, is shown in figure 8.

The effects of subsurface inhomogeneities and measurement errors are assumed to be small compared to the effects due to subsurface fractures. All of the anomalies are very small and are difficult to separate from background noise. The interpretations below are not necessarily unique.

1. Observation: The EM data (figs. 5 to 8) show a number of anomalies with wavelengths appropriate to thin subvertical conductors (McNeill, 1980). Some of the anomalies can be correlated from line to line.

   Interpretation: Anomalies that are interpreted as a NE-trending fracture or fracture zone showed positive correlation peaks, between adjacent lines, near the intersections of the interpreted fracture with the east-striking lines (#1 on fig. 8).

2. Observation: A large anomaly on the northwest line (fig. 6) correlates well with some of the anomalies seen on the east-trending lines (fig. 5).

   Interpretation: The large anomaly on the northwest line is consistent with the interpretation of a northeast fracture or fracture zone.

3. Observation: Small anomalies on the east-trending lines and the northeast-trending line can be correlated.

   Interpretation: Anomalies present on the northeast and east lines may be related to a fracture or a fracture zone of northwestern orientation (#2 on fig. 8).

4. Observation: Small anomalies are present on the two northernmost east-trending lines and the easternmost north-trending line (fig. 7).

   Interpretation: These three anomalies could indicate another northwest-trending fracture or fracture zone in the northeastern corner of the study area (#3 on fig. 8).

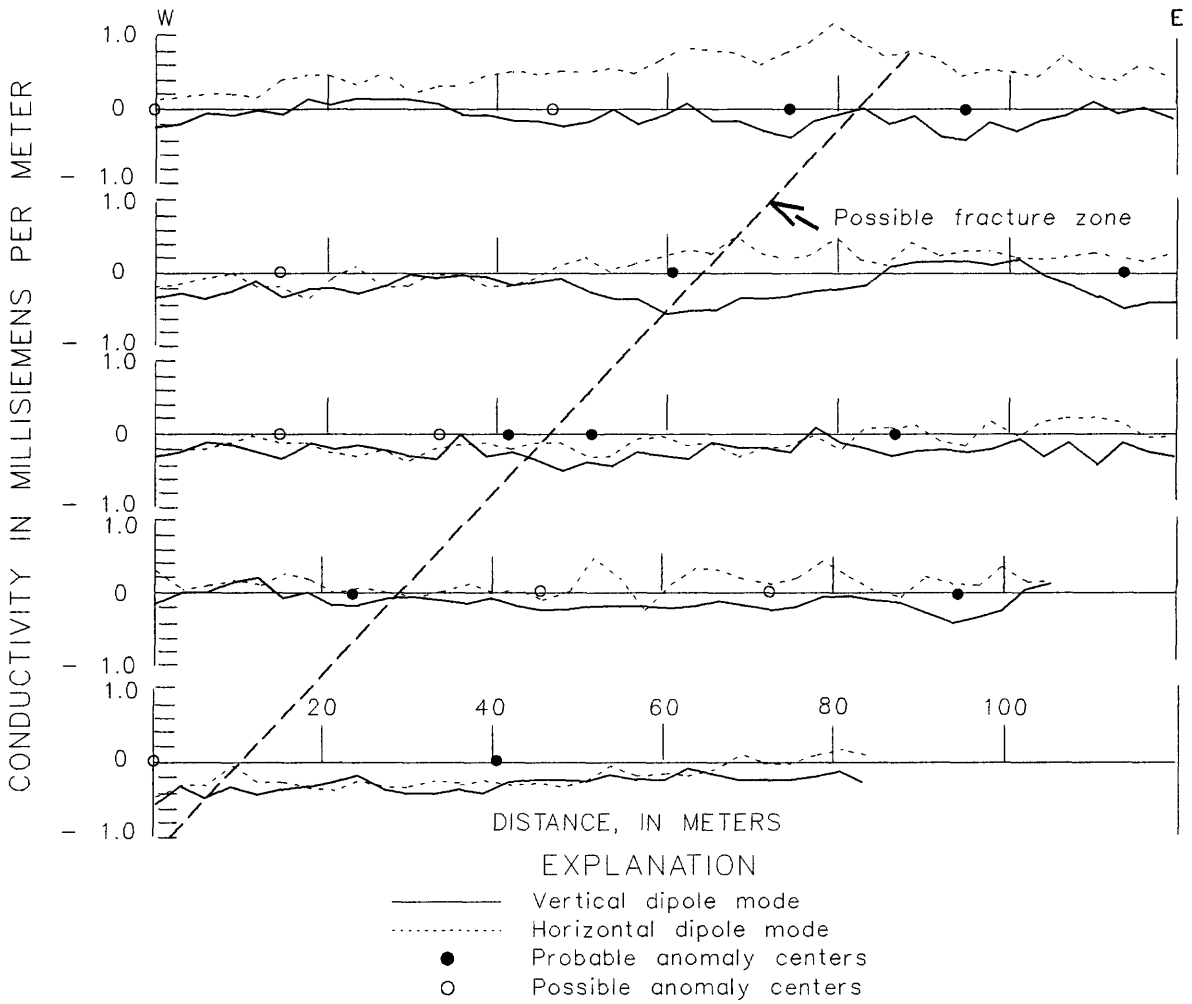

Figure 5.--Plot of inductive terrain-conductivity data--east lines.

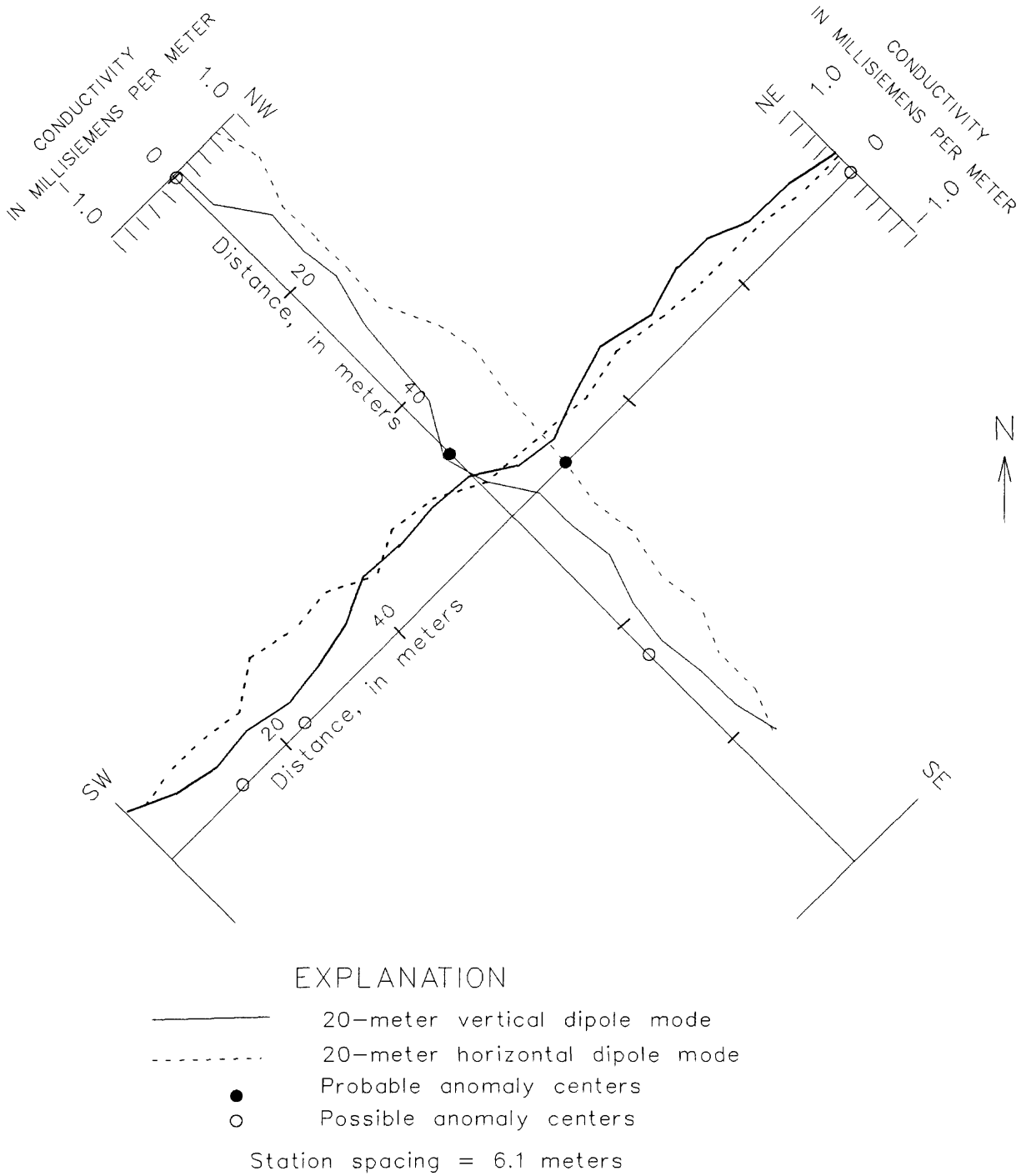

Figure 6.--Plot of inductive terrain-conductivity data--northeast and northwest lines.

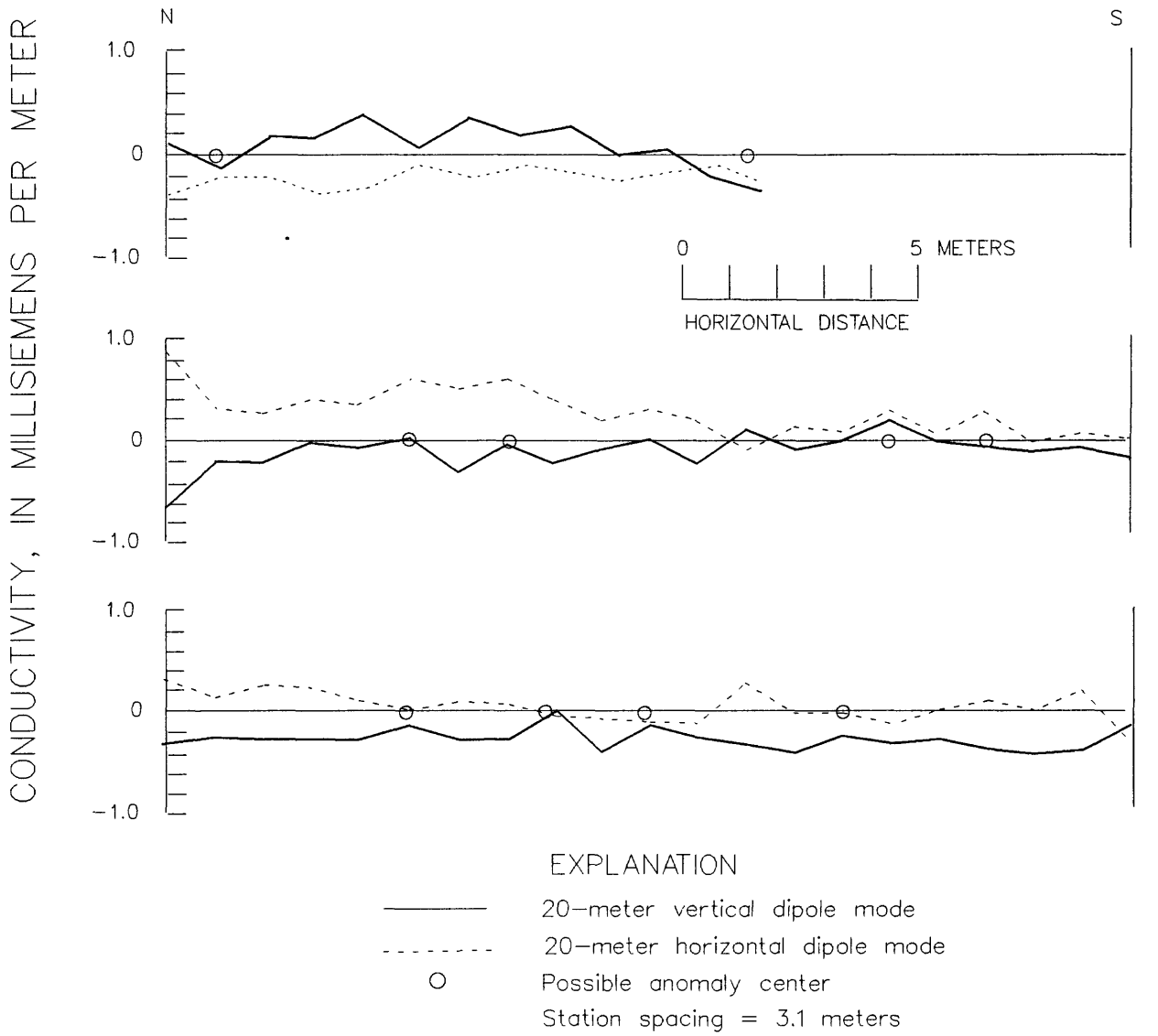

Figure 7.--Plot of inductive terrain-conductivity data--north lines.

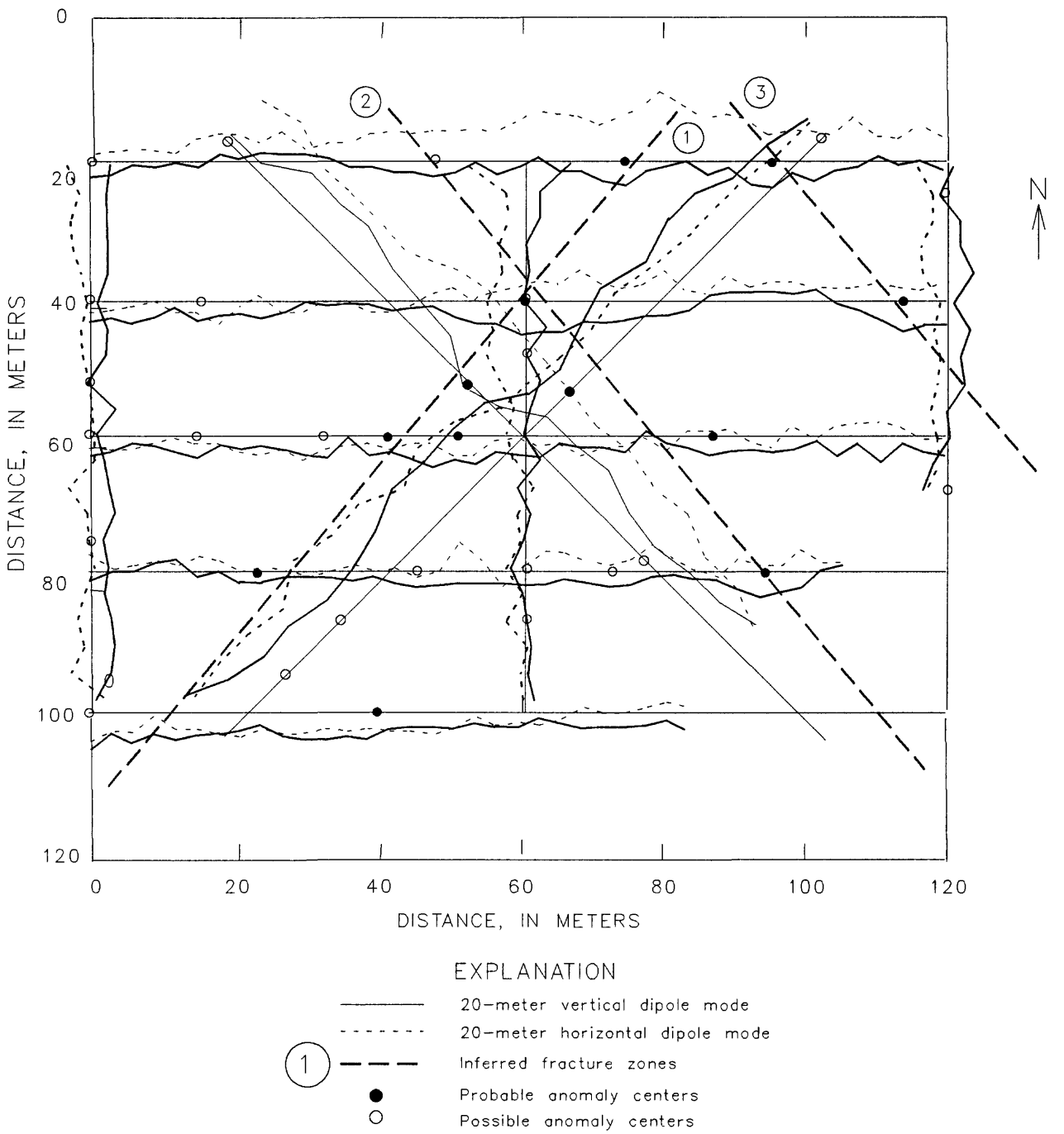

Figure 8.--Plot of inductive terrain-conductivity data--composite of all lines.

Direct-Current Resistivity

Data were collected in a standard Schlumberger array: A pair of current electrodes enclose a pair of voltage electrodes located on the same line and with a common center point. The current electrode spacing (AB) is large compared to the voltage electrode spacing (MN) and is progressively enlarged while the voltage electrode spacing is increased only to maintain a measurable potential. Soundings for AB/2 from 3 m to 80 m and MN/2 from 0.5 to 4 m were collected with the Bison 2390 earth resistivity instrument. The soundings were spaced 22.5° apart in azimuth. Plots of smoothed but unshifted field apparent resistivities as a function of azimuth for each current electrode spacing are shown in figures 9 to 14. The anisotropy quotient, defined here as the ratio of the maximum to the minimum apparent resistivity, is given as a measure of the maximum departure from an isotropic earth.

Noise contributions to the data included telluric currents (the effects of which are reduced significantly by a current reversal and stacking procedure performed in the instrument) and local near-surface resistivity variations near either the current or the voltage electrodes, or both.

The criteria used to determine the most significant orientation at a given AB/2 and MN/2 included a measure of significance and, where applicable, a measure of precision. For a given AB/2 and MN/2 spacing, an average apparent resistivity was calculated from all azimuthal measurements. The significance of a given orientation was determined by calculating its deviation from this average value. The most significant orientation, at a given AB/2 and MN/2 spacing, is defined as the orientation with maximum deviation from the average value. It is particularly important when the maximum and minimum resistivities are not separated by 90°. In addition, for AB/2 with two MN/2 spacings, precision was measured by the magnitude of the change in apparent resistivity between voltage-electrode spacings, for a given azimuth, at a given AB/2, as compared to the average change over all azimuths.

Observations and Interpretations

It is assumed that the complex patterns displayed in the azimuthal plots are significant, and the contribution from causes other than subsurface fractures is small. Despite this, the interpretation procedure was simplified by focusing on the most significant (as defined above) orientation at each AB/2, thereby reducing the complexity. The orientations of lower significance, which show up consistently, are also noted.

Other factors which may contribute to the observed azimuthal variation of resistivity include resistivity variations near the current and (or) voltage electrodes, telluric currents, the departure of the subsurface from horizontal homogeneous plane layering (foliation).

1. Observation: The azimuthal variation of resistivity is complex at all measured current electrode spacings (AB/2) (figs. 9 to 14).

   Interpretation: The data require more than one fracture set. Two interpretations of the complex azimuthal patterns are possible:

   a. The polar plots represent simple interference composites in which the directions of the azimuthal resistivity maxima correspond directly to fracture orientations.

   b. The polar plots represent complex interference composites from multiple fracture sets, which bear no simple direct relation to the orientations of subsurface fractures but are related to the most electrically conductive pathways through the rock. If this is the case, no simple interpretation method is available at this time. Important properties of single or multiple fracture sets that control the resulting azimuthal resistivity variation are: orientation, density, saturation, mean length, and depth range.

2. Observation: The anisotropy quotient is 1.2 to 1.9.

   Interpretation: The values of anisotropy, obtained here, compare well to the tabulated results of studies in other areas (Risk, 1975; McDowell, 1979; Palacky and others, 1981; Soonawala and Dence, 1981; Taylor, 1982; Mallik and others, 1983; Leonard-Mayer, 1984a, 1984b; Ogden and Eddy, 1984; Taylor, 1984; Taylor and Fleming, 1988).

3. Observation: At AB/2 spacings from 3 to 30 m (figs. 9 to 13), the NNE orientation, indicated by the maxima, is the most significant based on the criteria above. Other orientations of significance include ESE and ENE. The prominence of other secondary orientations decreases with depth. It should be noted that the absolute maxima and minima indicated on the figures sometimes differ from those used to determine the significant orientation: if the change in apparent resistivity from one voltage-electrode spacing to another, for a given AB/2, deviates significantly from the average change, a voltage electrode anomaly is assumed to be present and a correction is applied.

   Interpretation: A fracture set striking NNE is indicated. The ESE and ENE orientations, which decrease in prominence with increasing AB/2, may reflect the orientations of other fracture sets.

4. Observation: At 60- and 80-m AB/2 spacings (fig. 14), the north orientation, indicated by the maxima, is the most significant, although only six of the eight azimuthal measurements were made at these spacings. The north orientation also is the most significant at the 40-m AB/2 spacing (fig. 13); however, the NNE orientation is also significant. It is unclear which of the two orientations, N or NNE, is the most significant at this spacing because apparent resistivity measurements are of low precision on three of the azimuths.

   Interpretation: A fracture set striking north is indicated. This may represent a second set which is present at greater depths than the first and which replaces the first or, it may reflect a rotation of the formerly NNE striking set to the north at depth.

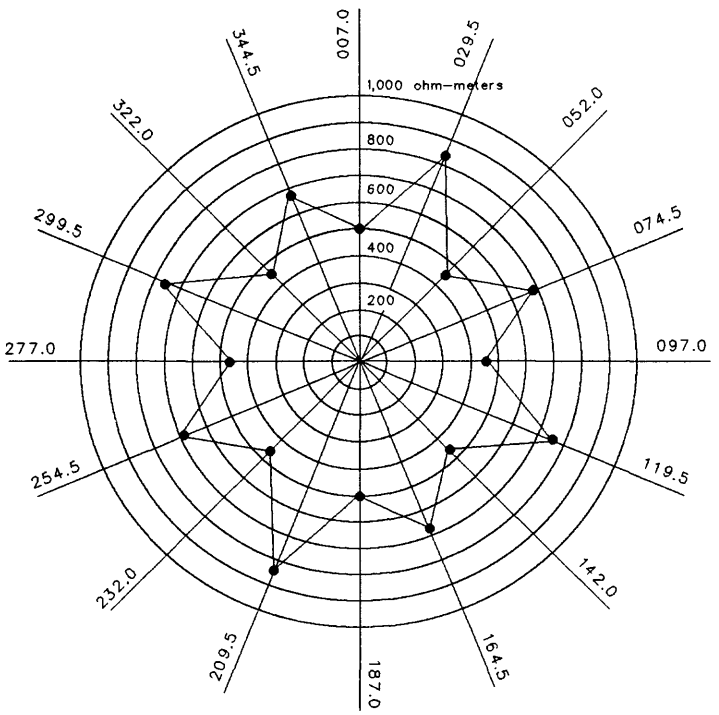

AB/2 = 3.00 meters

EXPLANATION

• Apparent azimuthal resistivity in ohm-meters

——— MN/2 = 0.50 meters

007.0 = Degrees from magnetic north

Anisotropy quotient

822/466 = 1.76

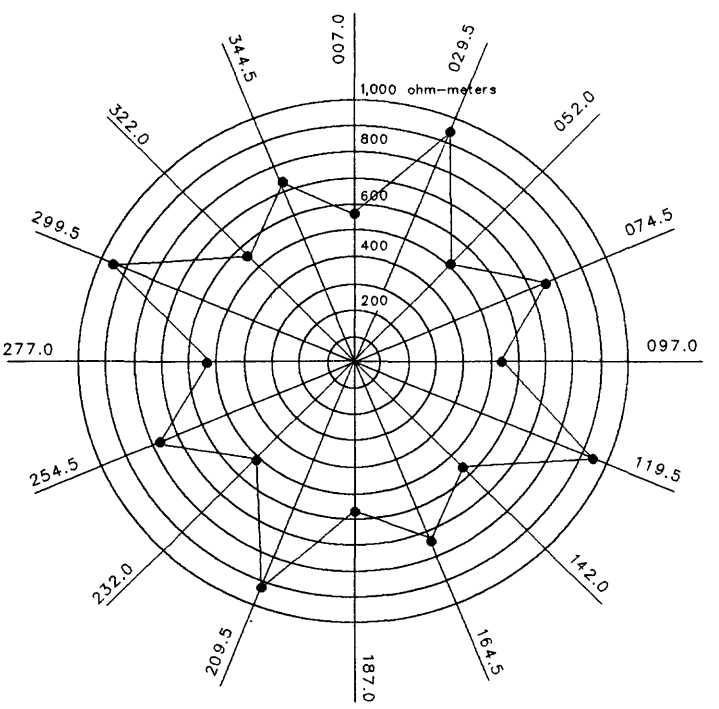

AB/2 = 4.00 meters

EXPLANATION

• Apparent azimuthal resistivity in ohm-meters

——— MN/2 = 0.50 meters

007.0 = Degrees from magnetic north

Anisotropy quotient

945/505 = 1.87

Figure 9.--Azimuthal plots of apparent resistivity for half-current electrode spacings of 3 and 4 meters.

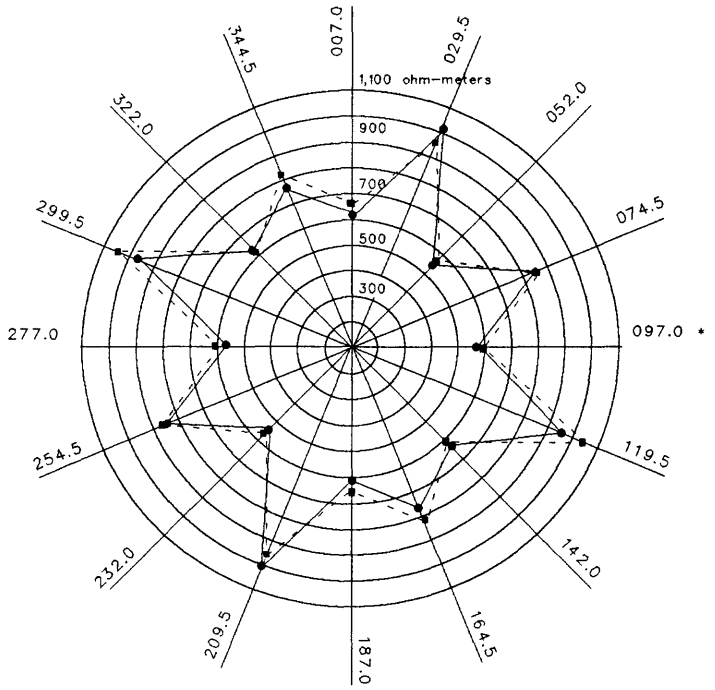

AB/2 = 5.00 METERS

EXPLANATION

• Apparent azimuthal resistivity in ohm-meters

——— MN/2 = 0.50 meter

- - - MN/2 = 1.00 meter

007.0 = Degrees from magnetic north

Anisotropy quotient

MN/2 = 0.50 meter: 1,003/540 = 1.85

MN/2 = 1.00 meter: 1,040/564 = 1.84

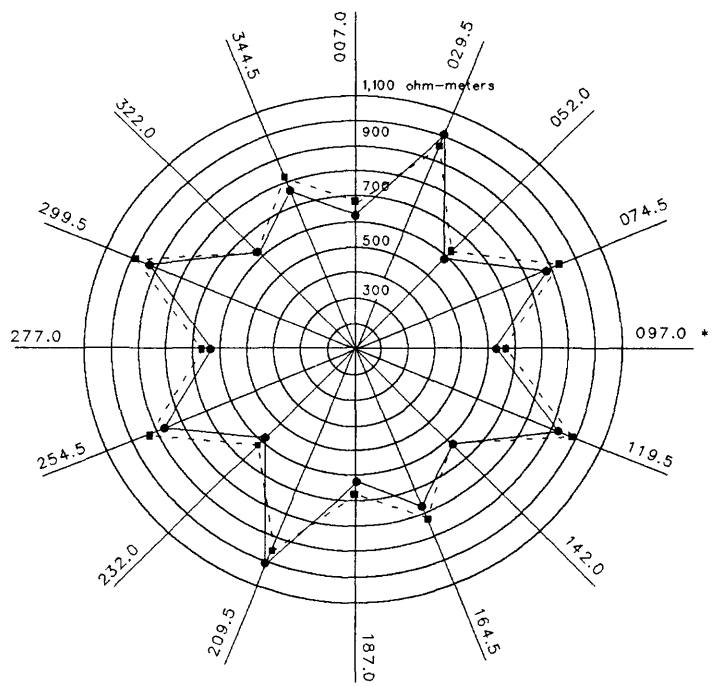

AB/2 = 6.00 METERS

EXPLANATION

• Apparent azimuthal resistivity in ohm-meters

——— MN/2 = 0.50 meter

- - - MN/2 = 1.00 meter

007.0 = Degrees from magnetic north

Anisotropy quotient

MN/2 = 0.50 meter: 1,038/595 = 1.74

MN/2 = 1.00 meter: 1,003/616 = 1.63

Figure 10.--Azimuthal plots of apparent resistivity for half-current electrode spacings of 5 and 6 meters.

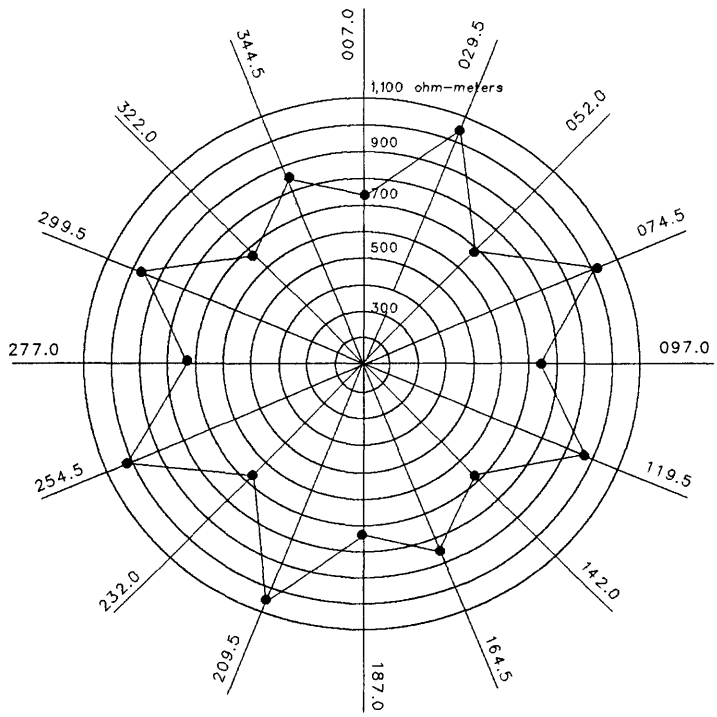

AB/2 = 8.00 meters

EXPLANATION

• Apparent azimuthal resistivity in ohm-meters

——— MN/2 = 1.00 meter

007.0 = Degrees from magnetic north

Anisotropy quotient
1,050/688 = 1.52

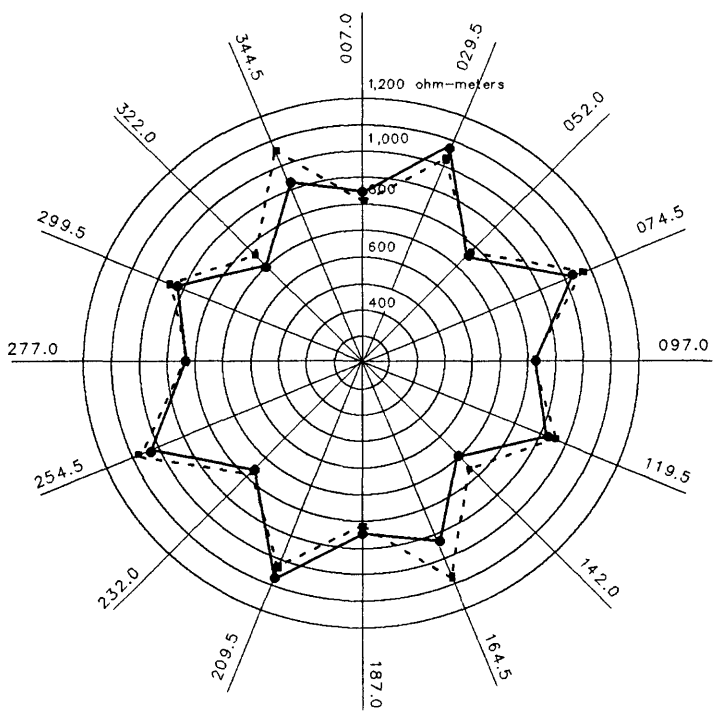

AB/2 = 10.00 meters

EXPLANATION

• Apparent azimuthal resistivity in ohm-meters

——— MN/2 = 1.00 meter

- - - MN/2 = 2.00 meters

007.0 = Degrees from magnetic north

Anisotropy quotient
MN/2 = 1.00 meter: 1,076/700 = 1.54
MN/2 = 2.00 meters: 1,082/758 = 1.43

Figure 11.--Azimuthal plots of apparent resistivity for half-current electrode spacings of 8 and 10 meters.

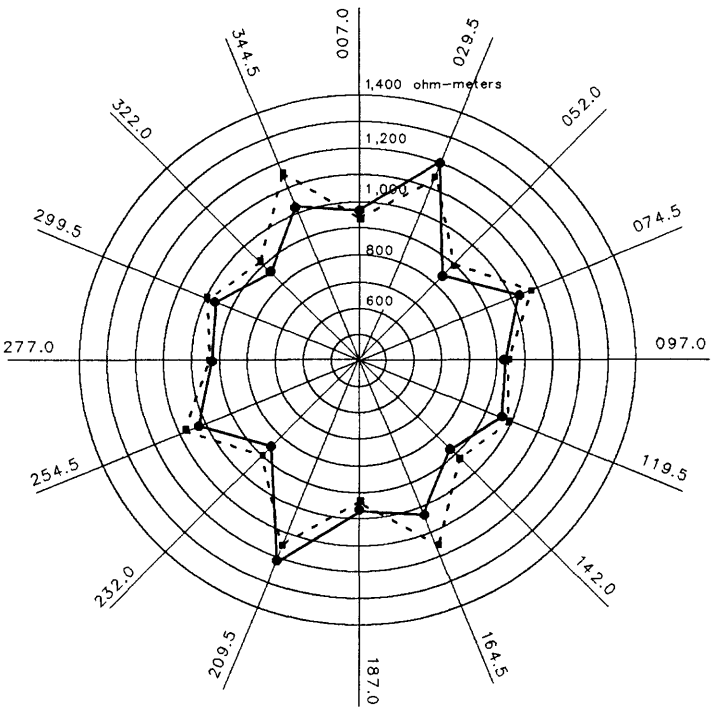

AB/2 = 14.00 meters

EXPLANATION

• Apparent azimuthal resistivity in ohm-meters

——— MN/2 = 1.00 meter

- - - - - - MN/2 = 2.00 meters

007.0 = Degrees from magnetic north

Anisotropy quotient

MN/2 = 1.00 meter: 1,201/850 = 1.41

MN/2 = 2.00 meters: 1,154/900 = 1.28

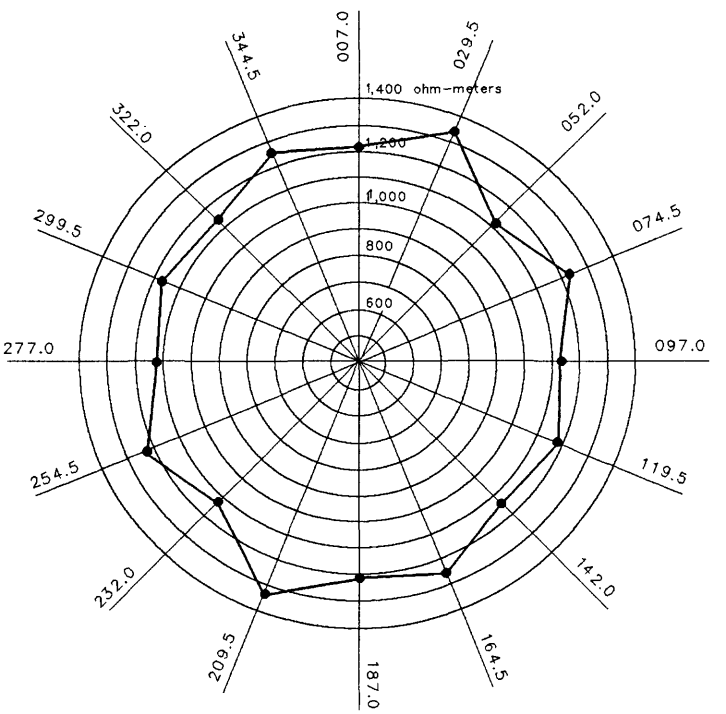

AB/2 = 20.00 meters

EXPLANATION

• Apparent azimuthal resistivity in ohm-meters

——— MN/2 = 2.00 meters

007.0 = Degrees from magnetic north

Anisotropy quotient

1,347/1,108 = 1.21

Figure 12.--Azimuthal plots of apparent resistivity for half-current electrode spacings of 14 and 20 meters.

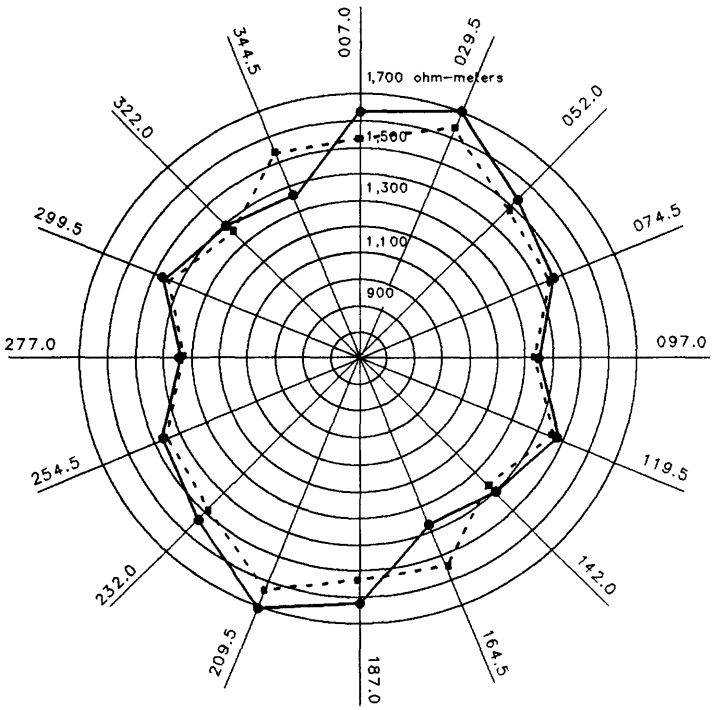

AB/2 = 30.00 meters

EXPLANATION

● Apparent azimuthal resistivity in ohm-meters

——— MN/2 = 2.00 meters

- - - - - - MN/2 = 4.00 meters

007.0 = Degrees from magnetic north

Anisotropy quotient

MN/2 = 2.00 meters: 1,706/1,341 = 1.27

MN/2 = 4.00 meters: 1,638/1,348 = 1.22

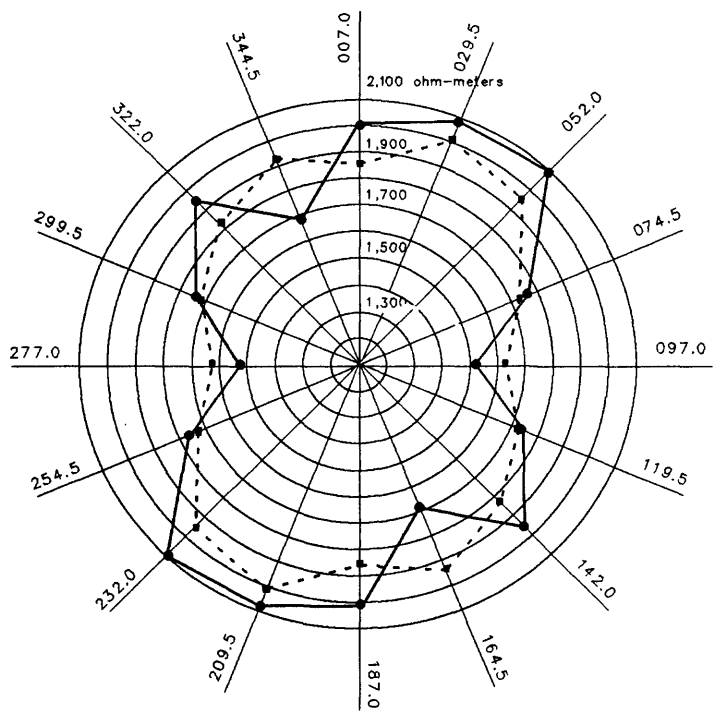

AB/2 = 40.00 meters

EXPLANATION

● Apparent azimuthal resistivity in ohm-meters

——— MN/2 = 2.00 meters

- - - - - - MN/2 = 4.00 meters

007.0 = Degrees from magnetic north

Anisotropy quotient

MN/2 = 2.00 meters: 2,100/1,523 = 1.38

MN/2 = 4.00 meters: 2,006/1,620 = 1.24

Figure 13.--Azimuthal plots of apparent resistivity for half-current electrode spacings of 30 and 40 meters.

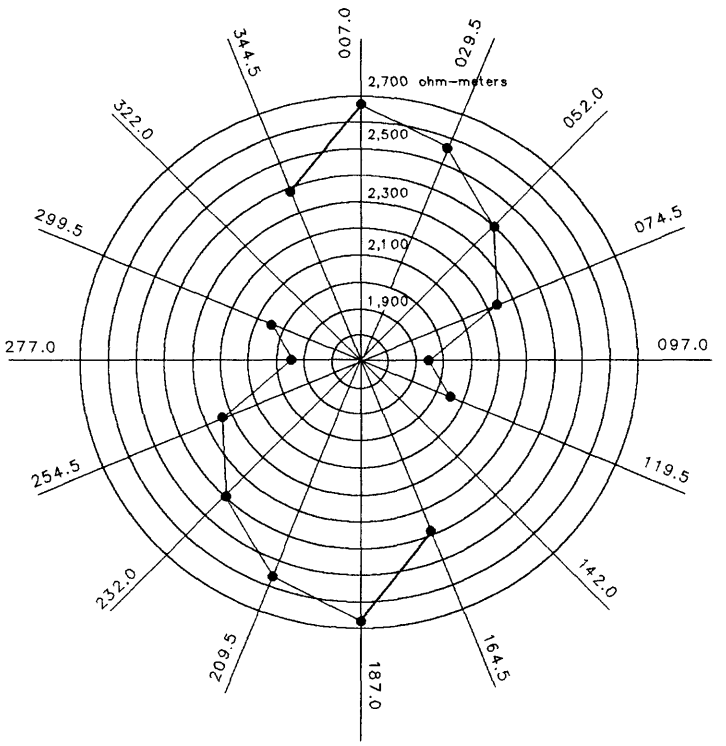

AB/2 = 60.00 meters

EXPLANATION

• Apparent azimuthal resistivity in ohm-meters

——— MN/2 = 4.00 meters

007.0 = Degrees from magnetic north

Anisotropy quotient

2,673/1,942 = 1.37

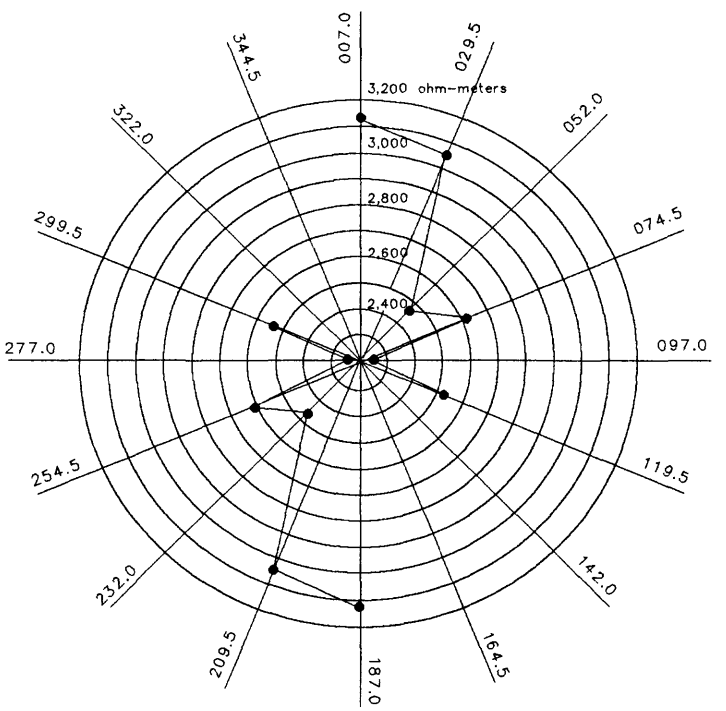

AB/2 = 80.00 meters

EXPLANATION

• Apparent azimuthal resistivity in ohm-meters

——— MN/2 = 4.00 meters

007.0 = Degrees from magnetic north

Anisotropy quotient

3,134/2,219 = 1.41

Figure 14.--Azimuthal plots of apparent resistivity for half-current electrode spacings of 60 and 80 meters.

5. Observation: At AB/2 spacings where azimuthal measurements were obtained for each of two MN/2 spacings, the azimuthal plots sometimes cross.

   Interpretation: The difference between the apparent resistivity values, obtained for the same current-electrode spacing and two different voltage-electrode spacings, on a given line, is related to the precision of the measurement and the effects of local subsurface inhomogeneities near the voltage electrodes. Where the change on a given line is close to the average change, the effect of local inhomogeneities is likely to be small. However, the variation of local inhomogeneities from line to line (azimuth to azimuth) may still be the dominant contribution to the observed crossing of the two azimuthal plots obtained at different voltage-electrode spacings. Alternatively, the measurement precision may be the dominant contribution.

Seismic Refraction

Seismic-refraction data using p-waves were acquired by rotating the line in 45°increments about a common center point. For each line, dynamite charges, buried approximately 15 m beneath the surface, served as the energy source at each shot location. Twelve vertical-displacement 7-Hz geophones were used as receivers. The geophones were spaced 6.1 m apart and there were five shots per line. The near end-shot was 10.7 m from the closest geophone, and the far end-shot was 44.2 m from the closest geophone. A center shot was used in order to obtain data on the depth of the water table. An EG&G 1210F signal-enhancement seismograph was used to record the data. Elevations were recorded for each shot location and each geophone position to within 0.03 m. Sound source depths and the depths to the water table in the shot holes also were recorded.

Unlike some of the other geophysical methods used in this study, plots of refraction field data do not easily convey information on p-wave velocity; analysis and interpretation must be performed prior to obtaining p-wave velocity, for a given line direction. Because the interpretation of fracture orientations may change depending on the results of the velocity analysis, the observation section contains a comparison of results obtained from a number of different interpretation methods. The results are presented as azimuthal velocity plots where each value is the result of a velocity analysis on the appropriately oriented refraction line. The different methods of velocity analysis are the linear regression method as implemented in the SIPT program (Haeni and others, 1987) and developed by Scott and others (1972) (fig. 15); the Hobson-Overton (HO) method as implemented in Haeni and others (1987) and developed by Scott and others (1972) (fig. 16); and the generalized reciprocal method (GRM) for XY=0 and the optimum XY (XY=30), as implemented by Stoyer (1987) and discussed in Palmer (1980) (figs. 17 and 18). The value of XY corresponds to the surface distance between the two rays emerging from the same refractor point and travelling towards opposite ends of the line. The XY value is important in velocity analysis and depth conversion.

Note that the use of the GRM in this report is an approximation. The GRM requires the measurement of reciprocal times and these surveys were not designed for the GRM; therefore, reciprocal times were linearly extrapolated from the measured data. Because velocity analysis is relatively insensitive to reciprocal time, this is not a problem. However, the results of depth conversion are sensitive to reciprocal time, and therefore no depth converted sections were produced based on the extrapolated data.

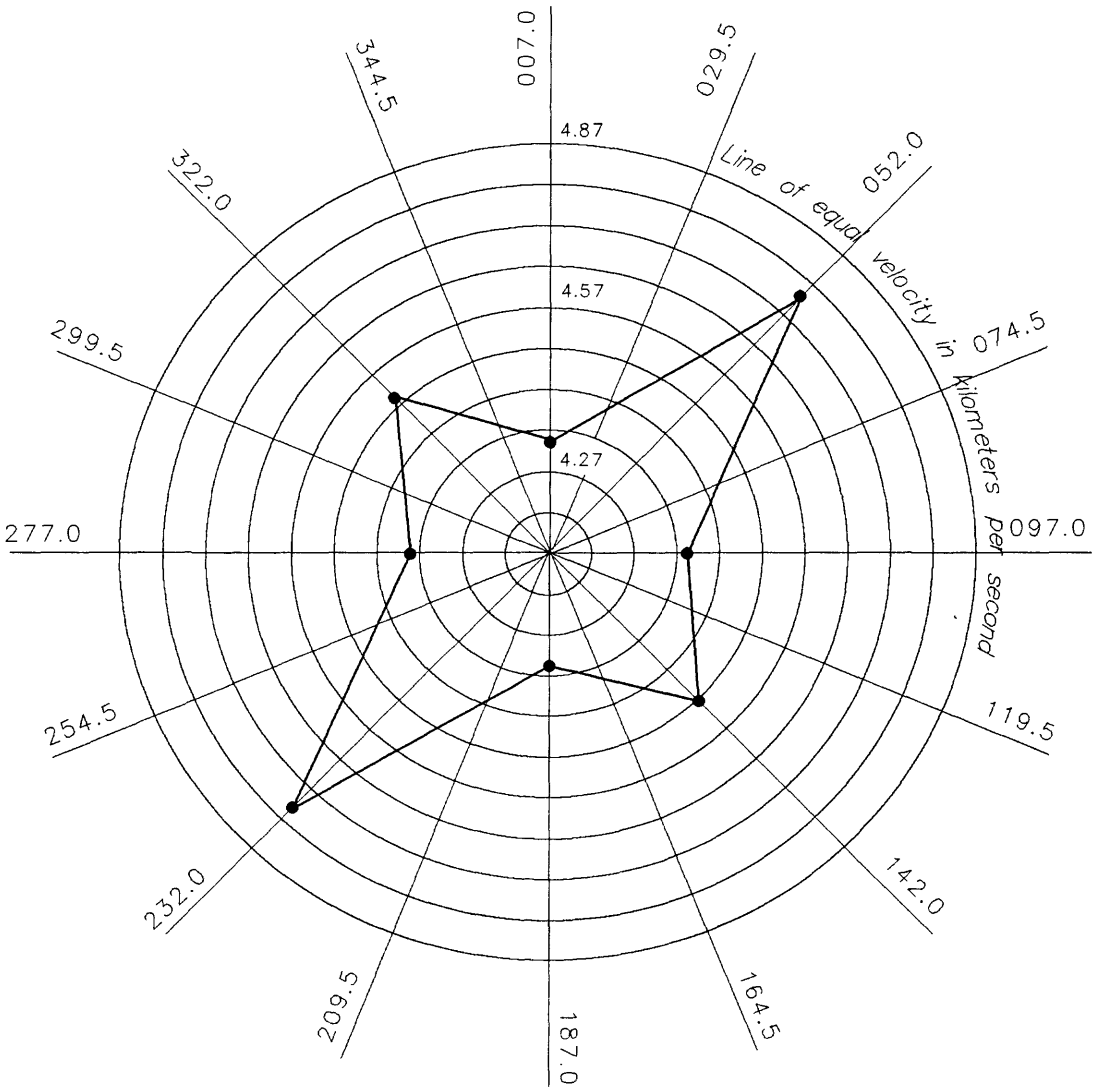

EXPLANATION

● Azimuthal p-wave velocity in bedrock

007.0 = Degrees from magnetic north

Anisotropy quotient

4.76/4.33 = 1.10

Figure 15.--Azimuthal plot of p-wave velocity in bedrock obtained by the linear-regression method of velocity analysis.

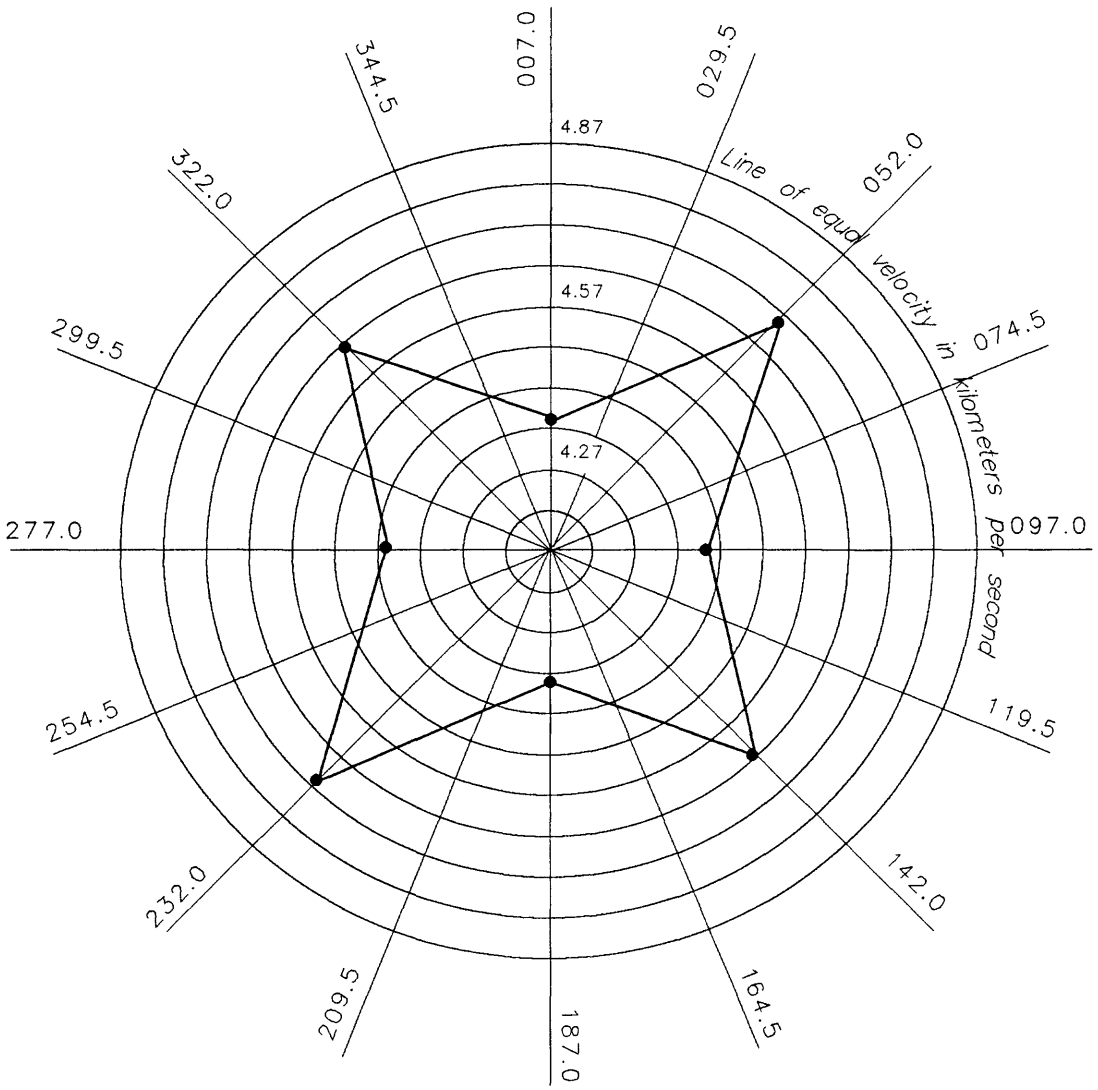

EXPLANATION

• Azimuthal p-wave velocity in bedrock

007.0 = Degrees from magnetic north

Anisotropy quotient

4.72/4.35 = 1.08

Figure 16.--Azimuthal plot of p-wave velocity in bedrock obtained by the Hobson-Overton method of velocity analysis.

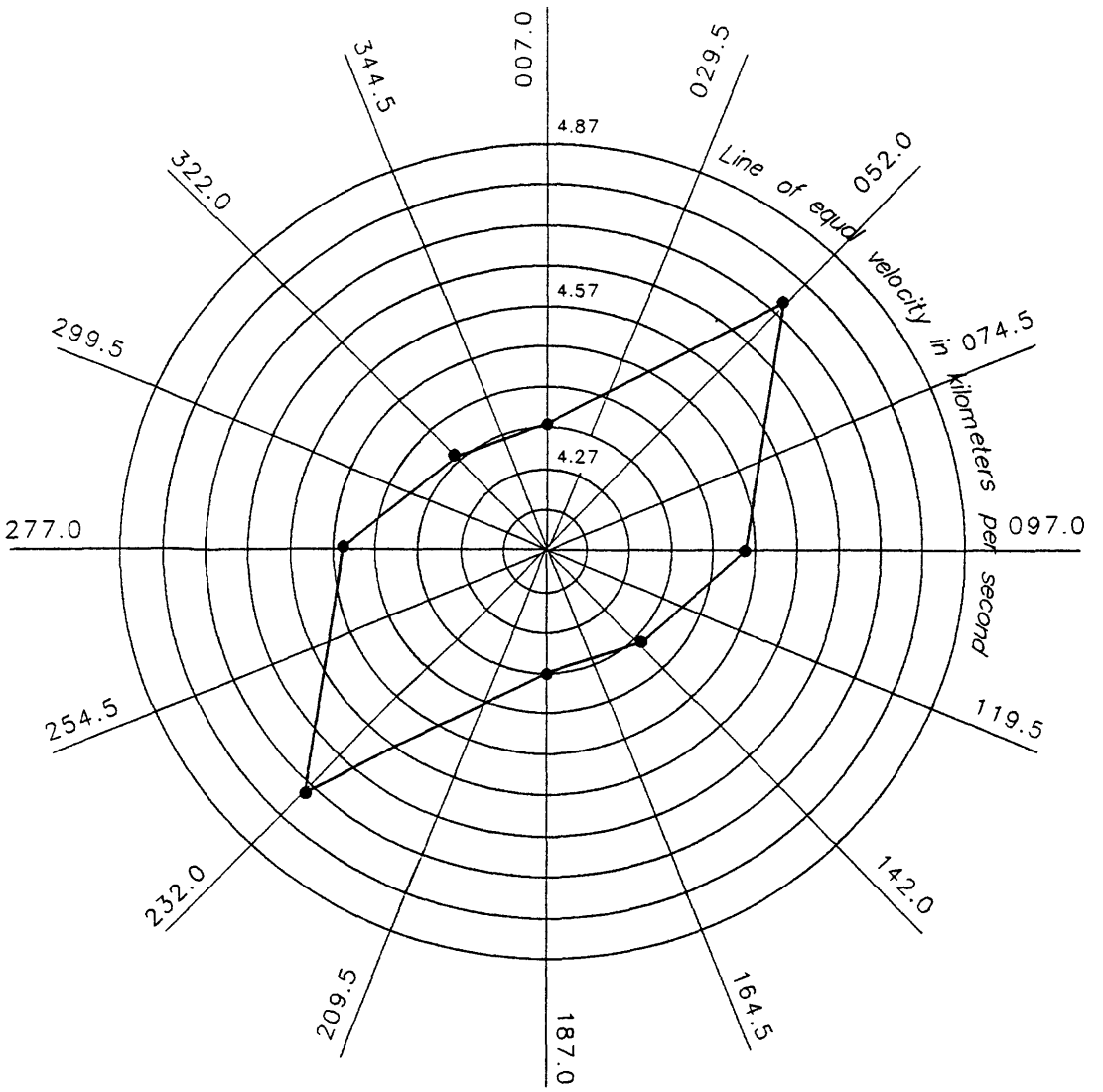

EXPLANATION

• Azimuthal p-wave velocity in bedrock

007.0 = Degrees from magnetic north

Anisotropy quotient

4.76/4.35 = 1.09

Figure 17.--Azimuthal plot of p-wave velocity in bedrock obtained by the the generalized reciprocal method of velocity analysis for XY=0.

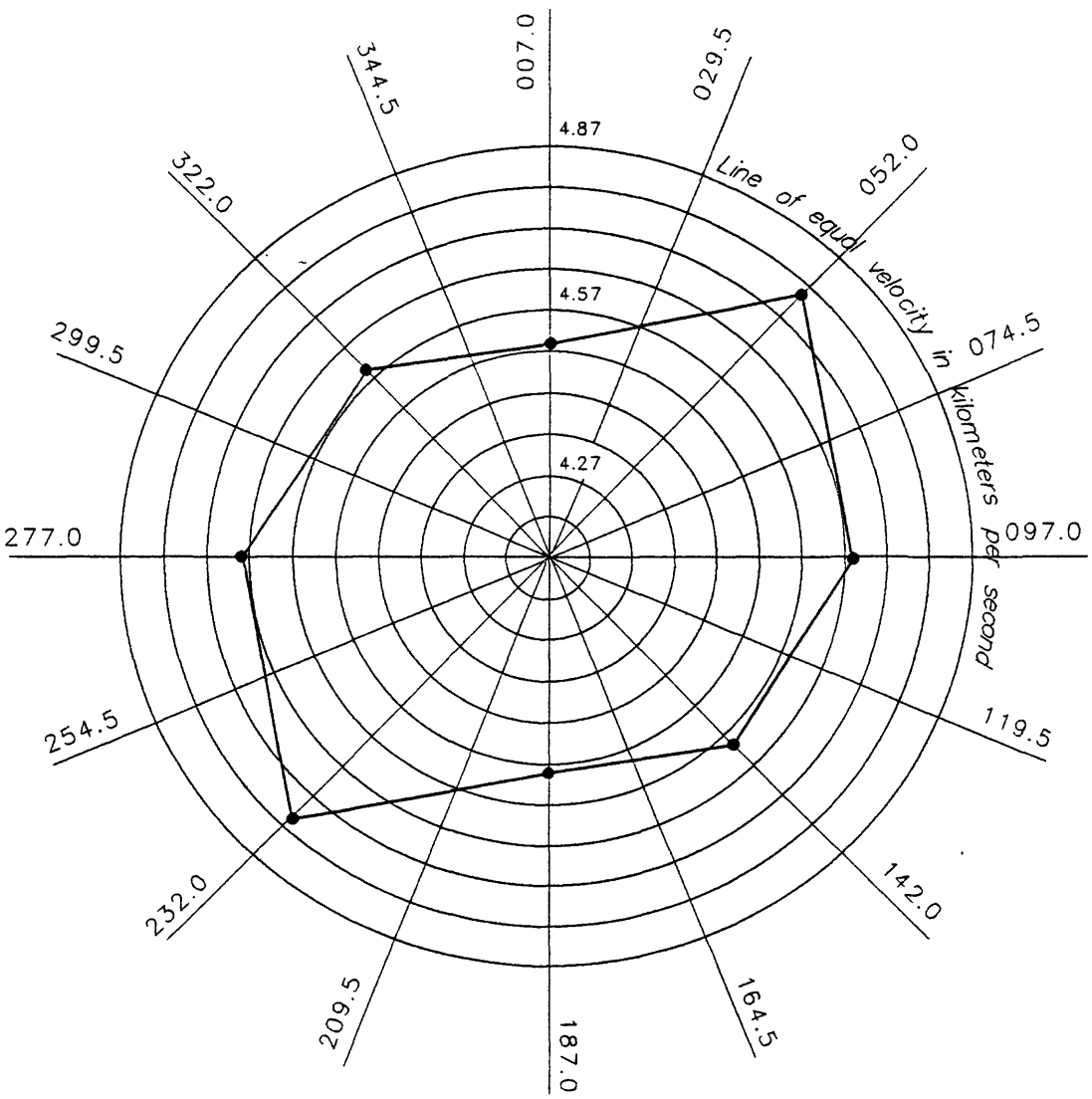

EXPLANATION

● Azimuthal p-wave velocity in bedrock

007.0 = Degrees from magnetic north

Anisotropy quotient

4.79/4.50 = 1.06

Figure 18.--Azimuthal plot of p-wave velocity in bedrock obtained by the generalized reciprocal method of velocity analysis for the optimum XY (XY=30).

Where the absolute maximum and minimum are not orthogonal, the maximum deviation from the average velocity was used to identify the most significant orientation.

Subsurface azimuthal anisotropy is assumed to play the primary role in determining the complexity of the azimuthal plots. Other factors which may contribute to the observed azimuthal variation of p-wave velocities include lateral variation of the p-wave velocity and the thickness of the first (overburden) layer, and p-wave velocity variations within bedrock.

The simplest interpretation of the velocity data uses the linear-regression method. This method makes a best-fit straight line through the arrival times from a designated layer. Large-scale variation in overburden thickness can be accounted for but was neglected in this implementation, inasmuch as the velocities obtained from opposing shots were averaged. Thickness changes and lateral variations in velocities are not accounted for if they occur on scales that are small compared to the line. The HO method (Scott and others, 1972; Scott, 1973) uses linear regression but applies it to delay time--a quantity that incorporates the reversed shots explicitly and is, therefore, a more refined method for calculating the velocity than simple regression.

Velocity analysis using the GRM method where XY=0 is reported to be similar to that using the HO method (Palmer, 1980, p. 7). The optimum GRM utilizes an optimum value of XY. (Optimum XY is the distance between surface geophones where refracted rays from reversed shots emerge from the same point on the refractor.) This method requires the field aquisition of reciprocal times, which could only be estimated in this study. In theory, the optimum GRM is the method least sensitive to velocity and thickness changes in the overburden and to change in the seismic velocity of the refractor. A comparison of the different methods of seismic-refraction data interpretations is given by Scott and Markiewicz (1990).

1. Observation: The most significant orientation, indicated by the maximum, obtained from the linear regression interpretation of p-wave velocities (fig. 15) is NE. A prominent velocity maximum also occurs oriented NW.

   Interpretation: The NE orientation obtained from the linear regression method (fig. 15) is interpreted to be the direction of a fracture set. The complexity of the plots may require more than one fracture set. The NW velocity maximum may represent a fracture set, but also could be accounted for by relief on the refractor. Depth interpretations using the SIPT program (Haeni and others, 1987) and GRM (Stoyer, 1987) indicate a bedrock high to the northwest. This relief is unaccounted for in the linear regression interpretation and may account for all or part of this velocity maximum.

2. Observation: The most significant orientation, indicated by the maximum, obtained from the HO interpretation of p-wave velocities (fig. 16) is NE. A prominent velocity maximum also occurs oriented NW.

   Interpretation: The interpretation in # 1. also applies to the HO results. The increased prominence of the NE orientation relative to the NW orientation, as compared to figure 15, probably reflects a better estimate of the velocity in each direction. The improved estimate results from the explicit incorporation of reversed times in the HO

least-squares analysis as opposed to the linear-regression method, which poorly accounts for the reversed times, after the least-squares analysis.

3. Observation: The most significant orientation, indicated by the maximum, obtained from the GRM, XY=0 interpretation of p-wave velocities (fig. 17) is NE.

   Interpretation: The results of the GRM method of velocity analysis, for XY=0 vary by less than 1 percent from those of the HO method for all directions except NW-SE. In this direction, the results varied by less than 5 percent. These results indicate that for XY=0, the GRM method is similar to the HO method, as reported by Palmer (1980, p. 7). The larger variation in the NW-SE direction is an indication that effects due to relief on the refractor surface are present. Depth sections indicate that this direction is closest to the dip direction of a refractor structure. Palmer (1980, p. 34) shows that where refractor topography is present, non-optimum XY values cause the time distance plot to deviate from a line. Velocity estimates at nonoptimum XY, differ from the optimum XY estimate because of this, especially if the number of points used to determine the line decreases between the optimum XY and the one used. Such changes are a normal consequence of doing velocity analysis using different XY values.

4. Observation: The most significant orientation, indicated by the minimum, obtained from the GRM, optimum XY (XY=30) interpretation of p-wave velocities (fig. 18) is north. The velocity maximum is oriented NE.

   Interpretation: Velocity analysis using the optimum XY on a given line is supposed to yield the most accurate measure of seismic velocity of subsurface layers. In a 12-geophone spread, the optimum XY is difficult to determine and the resulting velocity analysis is dependent on the chosen XY value. At the study site, the seismic velocity on the NE line was relatively independent of the XY value, while on the NW line, the seismic velocity was dependent on the XY value. This difference is interpreted to be the result of the topography on the refractor. This means that as the seismic line becomes parallel with the strike of the refractor (in the NE direction), the seismic velocity is less dependent on the chosen XY value. This indicates that the NW oriented maximum, found in both the regression and HO methods of velocity analysis, is probably due to uncompensated refractor topography. The easterly direction can be interpreted as the strike of a fracture set, indeed it is this direction which is indicated consistently by the absolute minimum obtained from each method. However, the absolute maxima, which are more significant than the minima for all but this method, indicates a NE striking fracture set. This interpretation can be extended to this method if the velocity in the NW direction remains abnormally high owing to an undercompensated topographic effect.

5. Observation: The anisotropy quotient, the ratio of the maximum to minimum interpreted azimuthal velocity, obtained from the different methods is as follows: linear regression=1.10; HO=1.08; GRM (XY=0)=1.09; GRM (XY=optimum)=1.06.

   Interpretation: The magnitude of anisotropy, also expressed as the anisotropy quotient, is comparable to that obtained in studies of other areas (Bamford and Nunn, 1979; Crampin and others, 1980; Park and Simmons, 1982; Imse and Levine, 1985).

Correlations Between Geophysical Data Sets

A NE-trending fracture set and (or) zone is indicated in the interpretation of inductive terrain-conductivity, DC-resistivity, and seismic-refraction data. There is a weaker correlation between the same three data sets that may show a NW trending fracture set and (or) zone in the study area. This orientation, however, is perpendicular to the strike of both overburden and bedrock structures as determined by the GPR and seismic-refraction methods, respectively. The overburden structure may explain the NW-oriented anomalies in the DC-resistivity data that decrease in strength with depth. These local geophysical results are consistent with the dominant regional NE-trending fractures obtained previously from field mapping on outcrops and photolineament analysis.

SUMMARY AND CONCLUSIONS

A study integrating four surface-geophysical methods was conducted to indicate the presence and estimate the orientations of steeply dipping subsurface fractures at a site near Milford, New Hampshire. The methods used were ground-probing radar, inductive terrain conductivity, DC resistivity, and seismic refraction.

Four radar lines penetrated up to 12 m of alluvial flood-plain and ice-contact sediments on parts of each record. No reflections or diffractions from fractures were recognized on the radar sections.

Interpretation of the inductive terrain-conductivity data indicates one fracture or fracture zone that trends NE, and possibly a second that trends NW. Alternatively, this data may reflect the presence of structural inhomogeneities in the subsurface.

The DC-resistivity data can be interpreted as indicating two fracture sets, one that trends NNE and one that trends generally north at greater depths. The effects of large and small scale inhomogeneities in the shallow subsurface may contribute to a WNW orientation.

The seismic-refraction data are interpreted as showing a fracture set trending NE-SW and may indicate a second or alternative zone that trends NW. Some component of the observed anisotropy may be caused by refractor topography, lateral variations in seismic velocity of the overburden, and assumptions in the velocity analysis.

It is possible to correlate the results of DC resistivity, inductive terrain conductivity, and seismic refraction. A NE-trending fracture set is consistent with the results of these three geophysical methods, as well as previous geologic outcrop data. Fracture sets or zones indicated by only one method may be interpreted several different ways. They could indicate separate fracture sets, a complex interference between different fracture sets or zones, the effect of noise, or the departure of the subsurface from simplifying assumptions.

Existing methods of data collection, analysis, and interpretation should be used with caution when they are applied to problems involving the detection of subsurface fracturing. A great deal more theoretical and empirical work is required to understand (a) the use of the different methods in fractured rock (b) the effect of nongeologic noise on the data and interpretation (c) the effects of assumptions associated with each geophysical method in the analysis and interpretation; and (d) the degree to which the correlation of multiple data sets can restrict the number of possible subsurface geologic interpretations even if some individual methods fail to detect anomalies attributable to fractures.

REFERENCES

Bamford, David, and Nunn, K.R., 1979, In-situ seismic measurements of crack anisotropy in the Carboniferous limestone of northwest England: Geophysical Prospecting, v. 27, p. 322-338.

BCI Geonetics, Inc., 1984, Bedrock fracture fabric analyses of the Savage Well, Grugnale Pit, and Milford Landfill hazardous waste study areas, report for New Hampshire Water Supply Pollution Control Commission: Laconia, New Hampshire, BCI Geonetics, 13 p.

Beres, Milan, Jr., and Haeni, F.P., 1991, Application of ground-penetrating-radar methods in hydrogeologic studies: Ground Water, v. 29, no. 3, p. 375-386.

Crampin, Stuart, McGonigle, Robert, and Bamford, David, 1980, Estimating crack parameters from observations of P-wave velocity anisotropy: Geophysics, v. 45, no. 3, p. 345-360.

Frazer, L.N., 1990, Dynamic elasticity of microbedded and fractured rocks: Journal of Geophysical Research, v. 95, no. B4, p. 4821-4831.

Haeni, F.P., Grantham, D.G., and Ellefsen, Karl, 1987, Microcomputer-based version of SIPT--A program for the interpretation of seismic-refraction data: U.S. Geological Survey Open-File Report 87-103A (text), 13 p. and 87-103B, 5¼-inch disk, MS-DOS compatible.

Imse, J.P., and Levine, E.N., 1985, Conventional and state of the art geophysical techniques for fracture detection: National Water Well Association Annual Eastern Regional Groundwater Conference, 2nd, Portland, Maine, 1985, Proceedings, p. 18-36.

Johnson, D.G., 1987, Use of ground-penetrating radar for determining depth to the water table on Cape Cod, Massachusetts, in First National Outdoor Action Conference on Aquifer Restoration and Ground Water Monitoring and Geophysical Methods, Las Vegas, Nevada, Proceedings: Dublin, Ohio, National Water Well Association, p. 541-554.

Keller, G.V., and Frischknecht, F.C., 1966, Electrical methods in geophysical prospecting: Oxford, England, Pergamon Press, 523 p.

Koteff, Carl, 1970, Surficial geologic map of the Milford quadrangle, Hillsborough County, New Hampshire: U.S. Geological Survey Geologic Quadrangle Map GQ-881, scale 1:62,500.

Leonard-Mayer, P.J., 1984a, A surface resistivity method for measuring hydrologic characteristics of jointed formations: U.S. Bureau of Mines Report of Investigations 8901, 45 p.

_____ 1984b, Development and use of azimuthal resistivity surveys for jointed formations, in Nielsen, D.M., and Curl, Mary, (eds.), National Water Well Association/U.S. Environmental Protection Agency Conference on Surface and Borehole Geophysical Methods in Ground-Water Investigations, San Antonio, Texas, Proceedings: Worthington, Ohio, National Water Well Association, p. 52-91.

Mallik, S.B., Bhattacharya, D.C., and Nag, S.K., 1983, Behaviour of fractures in hard rocks--A study by surface geology and radial VES method: Geoexploration, v. 21, p. 181-189.

McDowell, P.W., 1979, Geophysical mapping of water filled fracture zones in rocks: International Association of Engineering Geology Bulletin, v. 19, p. 258-264.

McNeill, J.D., 1980a, Electromagnetic terrain conductivity measurement at low induction numbers: Geonics Limited, Technical Note TN-6, 15 p.

McNeill, J.D., 1980b, EM34-3 survey interpretation techniques: Geonics Limited, Technical Note TN-8, 16 p.

Nair, R.M., Biswes, S.K., and Mazamdar, K., 1968, Experimental studies on the electromagnetic response of tilted conducting half-planes to a horizontal loop prospecting system: Geoexploration, v. 6, p. 207-244.

New Hampshire Water Supply and Pollution Control Commission, 1985, Hydrological investigation of Savage Well Site, Milford N.H.: Concord, N.H., 91 p.

Ogden, A.E., and Eddy, P.S., Jr., 1984, The use of tri-potential resistivity to locate fractures, faults and caves for siting high yield water wells, in Nielsen, D.M., and Curl, Mary, (eds.), National Water Well Association/U.S. Environmental Protection Agency Conference on Surface and Borehole Geophysical Methods in Ground-Water Investigations, San Antonio, Texas, Proceedings: Worthington, Ohio, National Water Well Association, Proceedings, p. 130-149.

Olsson, Olle, Andersson, P., Carlsten, S., Falk, L., Niva, Borje, and Sandberg, E., 1988, Fracture characterization in crystalline rock by borehole radar: Workshop on Ground Penetrating Radar, May 24-26, Ottawa, Canada, 24 p.

Palacky, G.J., Ritsema, I.L., and De Jong, S.J., 1981, Electromagnetic prospecting for groundwater in Precambrian terrains in the Republic of Upper Volta: Geophysical Prospecting, v. 29, p. 932-955.

Palmer, Derek, 1980, The generalized reciprocal method of seismic interpretation: Tulsa, Oklahoma, Society of Exploration Geophysicists, 104 p.

Park, Stephen, and Simmons, Gene, 1982, Crack induced velocity anisotropy in the White Mountains, New Hampshire: Journal of Geophysical Research, v. 87, no. 84, p. 2977-2983.

Risk, G.F., 1975, Detection of buried zones of fissured rock in geothermal fields using resistivity anisotropy measurements, in Geophysical papers submitted to the second U.N. symposium on the development and use of geothermal resources: San Francisco, California, May 20-29, p. 78-100.

Scott, J.H., 1973, Seismic refraction modeling by computer: Geophysics, v. 38, no. 2, p. 271-284.

Scott, J.H., and Markiewicz, R.D., 1990, Dips and chips--PC programs for analyzing seismic refraction data, in Symposium on the Application of Geophysics to Engineering and Environmental Problems, Golden, Colorado, Proceedings: Golden, Colorado, Society of Engineering and Mineral Exploration Geophysicists, 25 p.

Scott, J.H., Tibbetts, B.L., and Burdick, R.G., 1972, Computer analysis of seismic refraction data: U.S. Bureau of Mines Report of Investigation 7595, 95 p.

Soonawala, N.M., and Dence, M.R., 1981, Geophysics in the Canadian nuclear waste program--A case history: Society of Exploration Geophysicists Annual International Meeting, 51st, Los Angeles, Calif., 1981, Proceedings, p. 83-98.

Stewart, 1964, in BCI Geonetics report (1984) p.5 (no complete reference)

Stoyer, C.H., 1987, Gremix: Golden, Colorado, Interpex Ltd., 127 p.

Taylor, R.W., 1982, Evaluation of geophysical surface methods for measuring hydrological variables in fractured rock units: U.S. Bureau of Mines Research Contract Report, contract H0318044, 147 p.

_____ 1984, The determination of joint orientation and porosity from azimuthal resistivity measurements, in Nielsen, D.M., and Curl, Mary, (eds.), National Water Well Association/U.S. Environmental Protection Agency Conference on Surface and Borehole Geophysical Methods in Ground-Water Investigations, San Antonio, Texas, Proceedings: Worthington, Ohio, National Water Well Association, p. 37-49.

Taylor, R.W., and Fleming, A.H., 1988, Characterizing jointed systems by azimuthal resistivity surveys: Ground Water, v. 26, no. 4, p. 464-474.

Ulriksen, C.P.F., 1982, Application of impulse radar to civil engineering: Hudson, N.H., Geophysical Survey Systems, Inc., 179 p.

U.S. Environmental Protection Agency, 1985, Analysis of potential sources of groundwater contamination, Milford N.H.: Las Vegas, Nevada, Environmental Systems Monitoring Lab, TS-PIC-85-065, 29 p.

van Lissa, R.V., van Maanen, H.R.J., and Odera, F.W., 1987, The use of remote sensing and geophysics for groundwater exploration in Nyanza Province, Kenya: African Water Technology Conference, Nairobi, February 1987, 24 p.

Villegas-Garcia, C.J., and West, G.F., 1983, Recognition of electromagnetic overburden anomalies with horizontal loop electromagnetic survey data: Geophysics, v. 48, no. 1, p. 42-51.

Wait, J.R., 1990, Current flow into a three dimensionally anisotropic conductor: Radio Science, v. 25, no. 5, p. 689-694.

Yager, R.M., and Kappel, W.M., 1988, Detection and characterization of fractures and their relation to ground-water movement in the Lockport Dolomite, Niagara County, New York, in 3rd Annual Groundwater Technology Conference: New York, New York, Proceedings, September 1988, 47 p.

★U.S GOVERNMENT PRINTING OFFICE:1992-700-336/60035